INVESTIGATING THE ROLE OF M AND P PATHWAYS

IN THE HUMAN BRAIN

DURING BINOCULAR RIVALRY

by

Irem Yildirim

A dissertation submitted to the Faculty of the University of Delaware in partial fulfillment of the requirements for the degree of Doctor of Philosophy in Psychological and Brain Sciences

Spring 2022

INVESTIGATING THE ROLE OF M AND P PATHWAYS

IN THE HUMAN BRAIN

DURING BINOCULAR RIVALRY

by

Irem Yildirim

Approved: _____
Tania Roth, Ph.D.
Chair of the Department of Psychological and Brain Sciences

Approved: _____
John Pelesko, Ph.D.
Dean of the College of Arts and Sciences

Approved: _____
Louis F. Rossi, Ph.D.
Vice Provost for Graduate and Professional Education and
Dean of the Graduate College

I certify that I have read this dissertation and that in my opinion it meets the academic and professional standard required by the University as a dissertation for the degree of Doctor of Philosophy.

Signed: _____

Keith A. Schneider, Ph.D.
Professor in charge of dissertation

I certify that I have read this dissertation and that in my opinion it meets the academic and professional standard required by the University as a dissertation for the degree of Doctor of Philosophy.

Signed: _____

Timothy J. Vickery, Ph.D.
Member of dissertation committee

I certify that I have read this dissertation and that in my opinion it meets the academic and professional standard required by the University as a dissertation for the degree of Doctor of Philosophy.

Signed: _____

Jasmin Cloutier, Ph.D.
Member of dissertation committee

I certify that I have read this dissertation and that in my opinion it meets the academic and professional standard required by the University as a dissertation for the degree of Doctor of Philosophy.

Signed: _____

Zhenghan Qi, Ph.D.
Member of dissertation committee

ACKNOWLEDGMENTS

TABLE OF CONTENTS

Appendix

LIST OF TABLES

LIST OF FIGURES

ABSTRACT

When two sufficiently different stimuli are presented to each eye, perception alternates between them. Known as binocular rivalry, it is an example where visual consciousness needs to resolve a competition. Here, I aimed at investigating the neural mechanism behind this phenomenon, focusing on the contribution of the two visual pathways. Magnocellular (M) and Parvocellular (P) pathways are two information processing streams whose functions have been informative to explain many visual phenomena and clinical disorders. In the lateral geniculate nucleus (LGN), the M and P neurons are disjoint in a layered structure, receiving input from a single eye. Using magnetic resonance imaging (MRI), my goal was to identify the M and P layers in the LGN and examine the rivalry-related eye-specific responses within these layers. Series of techniques and analyses revealed that quantitative MRI is promising to identify the M and P layers in the LGN while functional MRI with monocular eye stimulation results in a clustered eye-specific structure and is not useful to separate the eye-specific regions into M and P sections. However, unsupervised approximation of the data with non-negative matrix factorization provided more consistent eye-specific structure than the generalized linear model. In the investigation of binocular rivalry, achromatic gratings induced rivalry that was represented in the eye-specific layers, and overall rivalry magnitude was similar in the M and P sections. These results highlight the importance of design and analysis in the functional imaging of the LGN layers and contributes to the binocular rivalry literature by showing the perceptual resolution in the LGN with achromatic stimuli and within M and P sections.

Chapter 1

IDENTIFYING THE LAYERS OF HUMAN LATERAL GENICULATE NUCLEUS USING MAGNETIC RESONANCE IMAGING

1.1 Introduction

The lateral geniculate nucleus (LGN) is the visual relay in the thalamus (Nassi & Callaway, 2009; Skalicky, 2016). It receives projections from retinal ganglion cells, projects primarily to the primary visual cortex (V1), and also receives massive feedback from V1. The LGN has a laminar structure, with typically six monocular layers in humans, receiving input alternatingly from the contralateral or ipsilateral eye (Figure 1.1a). The four dorsal layers contain parvocellular (P) neurons while the two ventral layers contain magnocellular (M) neurons (Figure 1.1b), receiving input from the midget and parasol ganglion cells in the retina respectively. The M and P neurons in LGN differ in their functional roles (Maunsell, 1992; Merigan & Maunsell, 1993). The M neurons are specialized to encode coarse and transient visual characteristics, such as luminance (Shapley & Perry, 1986) and temporal frequency (Derrington & Lennie, 1984), while the P neurons are able to encode detailed and sustained characteristics such as color and form (Livingstone & Hubel, 1988).
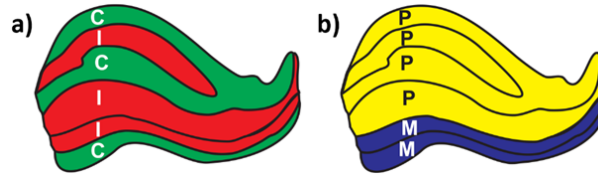
Figure 1.1:   The Structure of Lateral Geniculate Nucleus. M = Magnocellular, P = Parvocellular, C = Contralateral, I = Ipsilateral. Tracings were generated based on Andrews et al., (1997).

The M and P pathways are of considerable interest for their roles in the mechanisms of visual perception and consciousness (Breitmeyer, 2014; Denison & Silver, 2012; Milner, 2012) and in clinical disorders such as dyslexia (Stein, 2001; Stein & Walsh, 1997) and schizophrenia (e.g., Butler & Javitt, 2005; Schechter et al., 2003). Studying these pathways independently, however, has been challenging due to the intermixing of the two pathways starting in V1 (Aleci & Belcastro, 2016; Merigan & Maunsell, 1993). In the LGN, the M and P neurons are completely segregated in separate layers, but the small size of the LGN, with layers on the order of 1 mm thick, approaches the resolution limits of human neuroimaging. Previous MRI attempts have identified the layers at the group level and/or using a group-level criteria such as for the proportion of the M and P sections in LGN (Denison et al., 2014; Oishi et al., 2020; Zhang et al., 2015), but this does not enable the measurement of the properties of the M and P layers in individuals. Further, previous studies, such as Denison et al. (2014), Qian et al. (2020), and Zhang et al. (2015) attempted to identify the M and P layers with fMRI using visual stimuli tuned to the M or P neurons. However, DeSimone and Schneider (2019) showed that the hilum region of the LGN, a vascular region rich with blood vessels and nerves, had larger responses across the range of

2

stimuli. They found that any method based only on the response amplitudes without proper normalization would be likely to mistake the hilum for the M layers.

My aim was to be able to identify the M and P layers of the LGN in individual subjects using anatomical and/or functional procedures that did not rely upon their differences in functional response properties. Using fMRI, I aimed at identifying the contralateral layers of LGN, while leaving the bordering ipsilateral layers out (Figure 1.1a). Previously, Haynes et al. (2005) used monocular visual stimulation to separate the left eye and right eye signals but did not identify the M and P divisions. Qian et al. (2020) visually stimulated each eye with a dichoptic presentation and identified two clusters instead of layers, a lateral contralateral cluster and a medial ipsilateral cluster.

I sought to compare the fMRI results to structural methods. Recent developments in qMRI allow for measuring the microstructure of tissues (Lutti et al., 2014; Mezer et al., 2013) that can differentiate the M and P regions. The morphology of the M and P neurons in LGN differ with the P neurons having small bodies and thin axons and the M neurons having large cell bodies and thick axons. The cell density is therefore higher in the P layers (Hassler, 1966) and there is greater myelination in the P compared to the M layers (Pistorio et al., 2006). Müller-Axt et al. (2021) used a 7T MRI scanner and observed shorter T1 relaxation for the P region than the M region in LGN (also Oishi et al., 2020). I sought to replicate this technique at 3T.

1.2 Methods

1.2.1 Participants

The protocols for this study, together with the protocols for Chapter 3, were approved by the University of Delaware Institutional Review Board (see Appendices).

Three healthy participants (1 male and 2 female, age range = 28–33 years) were recruited and provided informed consent. They were compensated at a $20/hour rate for their participation. All participants reported normal or corrected-to-normal vision.

1.2.2 MRI Procedures and Processing

Each participant was scanned on seven different days (four structural scanning sessions and three functional) for approximately 90 min each day. MRI data were acquired on a 3T Siemens Magnetom Prisma MRI scanner with a 64-channel head coil. We used FSL software (https://fsl.fmrib.ox.ac.uk/fsl/fslwiki/FSL) to process all the MRI data unless otherwise noted.

1.2.2.1 T1-weighted MRI

At the beginning of each scanning session, we acquired a 3D MPRAGE sequence (0.7 mm isotropic voxels, repetition time (TR) = 2080 ms, echo time (TE) = 4.64 ms, inversion time (TI) = 1050 ms, flip angle (α) = 9°, field of view (FoV) = 210 mm, phase-encoding acceleration factor = 2, scan time approximately 6 min). All subsequent scans were aligned to the T1-weighted image of each subject's first session and analyzed in their native space.

1.2.2.2 Quantitative MRI (qMRI)

qMRI data were acquired with a 3D MP2RAGE sequence (0.7 mm isotropic voxels, TR = 5000 ms, TE = 3.6 ms, Partial Fourier in slice = 6/8, approximately 16 min acquisition time). The sequence had two inversion times and two flip angles (TI1 = 900 ms, TI2 = 2750 ms, $\alpha 1$ = 3°, $\alpha 2$ = 5°), enabling the calculation of the T1 relaxation time, i.e., qT1 map. Seventeen scans were acquired for each participant

during four sessions on different days, during which participants watched a movie of their choice.

The MP2RAGE sequence simultaneously acquired the T1-weighted (GRE_{TI1}) and proton density weighted (GRE_{TI2}) image volumes. The uniform T1-weighted image volume was obtained from the real component of the normalized complex ratio from the two acquired image volumes. This process amplifies the noise in the uniform T1-weighted image; the numeric instability in background noise was suppressed by introducing a constant real number (beta) to the uniform T1-weighted image volume (O'Brien et al., 2014). We computed qT1 maps, a measurement of the T1 relaxation constant for each voxel, using the MP2RAGE toolbox (https://github.com/benoitberanger/mp2rage) in SPM (https://www.fil.ion.ucl.ac.uk/spm/software/spm12/) in MATLAB. qT1 maps were computed for each of the 17 scans for each participant.

To create LGN masks, I used the 17 qT1 maps, 16 of which were aligned to the first one and averaged. The average qT1 map for each subject was then resampled to double the resolution (0.35 mm isotropic voxels), with a sinc interpolation. Using this upsampled qT1 map, I manually masked each LGN for each participant (Figure 1.3a). The upsampled qT1 map and LGN mask were then aligned to their initial T1 image.

To identify the M and P sections, the average qT1 map for each participant was masked for their left and right LGN (Figure 1.3b) and analyzed separately. As there should be M and P parts differing in their qT1 value within the LGN (Müller-Axt et al., 2021), I first fit each qT1 map to a mixture of two Gaussians. Figure 1.4a displays the histograms of qT1 maps with the fitted Gaussians. Next, I calculated the fraction

of M voxels to the right of the distribution, for a given qT1 value as the separation point (dark blue line in Figure 1.4a). Specifically, I multiplied the proportion of each component with the cumulative distribution function of the fitted Gaussian and took the ratio of this result for the component with the smaller proportion (i.e., the M component) to the sum of the results for both components. Then, I determined a cut-off qT1 value (dashed line in Figure 1.4a) as where this fraction was 0.5, indicating that at least 50% of the identified M set at this cut-off is M voxels. I decided to be lenient on this threshold because the M voxels had more variable qT1 values and were underestimated in the mixture Gaussian model. For example, when post-mortem LGN were analyzed, Müller-Axt et al. (2021) found less flat Gaussian fits for M with a similar analysis.

1.2.2.3   Functional MRI (fMRI)

fMRI data were acquired over the whole brain with a multi-band EPI sequence with 84 interleaved transversal slices at 1.5 mm isotropic voxel resolution (TR = 1500 ms, TE = 39 ms; α = 75°; FoV= 192 mm, bandwidth = 1562 Hz/Px, phase encoding = A → P), and a slice acceleration factor of 6.

1.2.2.3.1   LGN localizer

For each of ten 5-min scans, participants were instructed to fixate on the dot at the screen center. As shown in Figure 1.2a, a 5 s fixation screen was followed by the 16 s visual stimulus, that alternated between left and right hemifields always with a 5 s blank in between alternations. The initial hemifield was counterbalanced across blocks. Stimuli were presented on a 32-inch LCD BOLDscreen with a 60 Hz refresh rate and 1920×1080 resolution. The stimuli were prepared and presented in MATLAB

using Psychophysics Toolbox (Brainard, 1997) on a Windows computer. The visual stimulus was a black and white checkerboard, hemifield radius of 8.5°, flicking at 4 Hz on a neutral gray background. The fixation point was drawn within a central gap of 0.25° in radius.
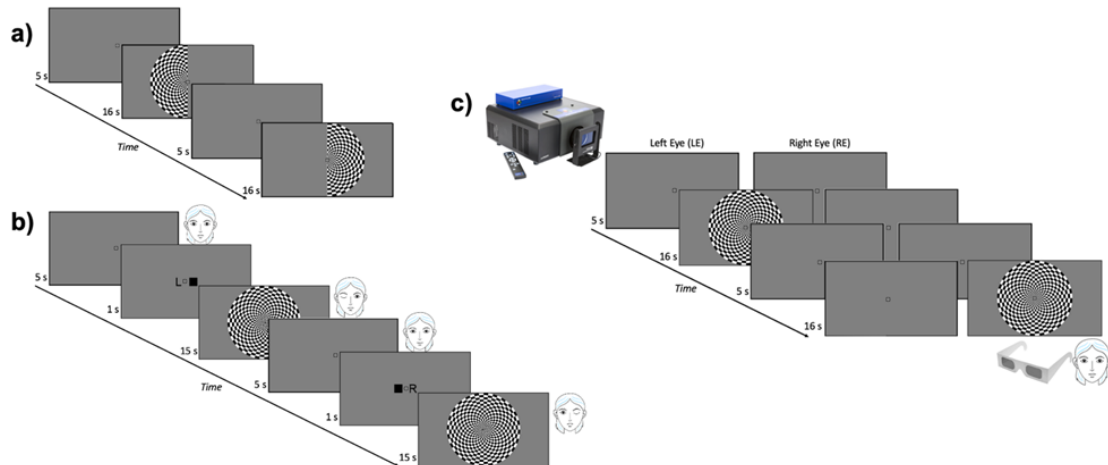
Figure 1.2:   Timeline of Localizer fMRI Tasks. a) LGN localizer with visual hemifield stimulation. b) Monocular eye localizer: each eye was stimulated alternately with the other eye closed. c) Dichoptic eye localizer: each eye was stimulated alternately with the other eye viewing a neutral gray blank screen.

1.2.2.3.2   Monocular Eye Localizer

For each of ten 5-min blocks (nine blocks for S2), participants were instructed to fixate on the central dot on the screen, and close one eye at a time when cued. A blank fixation screen was presented for 5 s followed by the instruction: the letter L (respectively, R) on the left (right) side of the central dot and a black square on the right (left) to indicate that the left (right) eye should be open and the right (left) eye closed (Figure 1.2b). After 1 s, the full-field 4 Hz flickering checkerboard (17°

diameter, 0.5° central gap) appeared for 15 s while the instruction remained in the central gap. The eye open conditions alternated regularly in a 5-minute block, with the order counterbalanced across different blocks. The software and the materials to prepare and present the stimuli was the same as those for the LGN localizer stimuli (see the previous Section 1.2.2.3.1).

1.2.2.3.3   Dichoptic Eye Localizer

Participants wore circularly polarized paper glasses, and stimuli were presented with a ProPixx (VPixx, Inc.) projector at 120 Hz refresh rate, 1920×1080 resolution, and a synchronized circularly polarizing filter in front of the projector lens, which allowed for dichoptic viewing at 60 Hz. As Figure 1.2c illustrates, the timeline of this task was the same as that of the LGN localizer, but with a full-field visual stimulus shown either to the left eye or to the right eye while the other eye was shown the neutral gray fixation screen. The flickering checkerboard stimulus was the same as in the monocular eye localizer task, except 12.5° in diameter, due to the different screen size. The stimuli were prepared using the DataPixx toolbox and Psychophysics toolbox in MATLAB, running on a Linux computer.

1.2.2.3.4   Data Processing

To pre-process the functional data, I applied motion correction using MCFLIRT, intensity normalization and high-pass temporal filtering. For the LGN localizer only, the data were spatially smoothed with a 2.5 mm FWHM kernel. We used the fsl_motion_outliers command to find the motion outlier volumes, thresholded at the 75th percentile + 1.5 times the interquartile range.

The data were analyzed with a generalized linear model (GLM) with two explanatory variables (EVs) for each experiment: left (LH) and right hemifield (RH) for the LGN localizer and left (LE) and right eye (RE) for the two eye localizer experiments. Also, a confound variable was added to the model for the motion outlier volumes. All the possible contrasts were computed between the two main EVs. The significance threshold for the LGN localizer was corrected for multiple comparisons using cluster correction whereas no correction was applied for the eye localizer tasks, as they were analyzed in the LGN region of interest defined by the localizer scans. Finally, I conducted a fixed-effects analysis for each participant to combine the multiple scanning runs from each task separately and in combination across tasks.

Before analyzing the eye-specific signals, I first adjusted the LGN masks based on the LGN localizer results. For each subject, I looked at the whole brain activity for LH vs RH and RH vs LH to find the right and the left LGN respectively. I outlined the LGN on the significant activity, using the LGN mask created from the anatomical qT1 map as an anchor in slice selection and border decision (Figure 1.3c). The reason for doing so was to make sure that I selected the area activated by the visual stimulus.

To identify the eye dominance signals in each LGN, the functional data from the monocular and the dichoptic eye localizer tasks were analyzed. For each voxel in the functionally adjusted LGN, I determined its ocular preference based on the t-score for the LE vs RE contrast, which was the measure of ocular preference that has been used in the literature (Haynes et al., 2005; Qian et al., 2020). A positive t-score indicated stronger LE response for the voxel whereas a negative value indicated stronger RE response.

1.3 Results

1.3.1 LGN volume

We calculated the LGN volume for each participant by using the LGN masks created from the anatomical qT1 map (Figure 1.3b). The left LGN was measured as 138.2, 132.4, and 131.0 mm^3 for each of three subjects and was smaller than their right LGN, measured as 147.2, 149.6, and 132.4 mm^3 respectively. We also calculated the LGN volumes using the LGN masks that were adjusted for the significant visual activity (Figure 1.3c). These functionally adjusted LGN masks resulted in volumes of 125.9, 124.9, and 116.6 mm^3 for the left LGN and 154.0. 114.9, 130.3 mm^3 for the right LGN, for each subject respectively. These volumes are smaller than the volumes that were calculated from the anatomically defined LGN, except for S1's right LGN. These volumes are within the range of 91 to 157 mm^3 that had been reported in a histology study (Andrews et al., 1997).
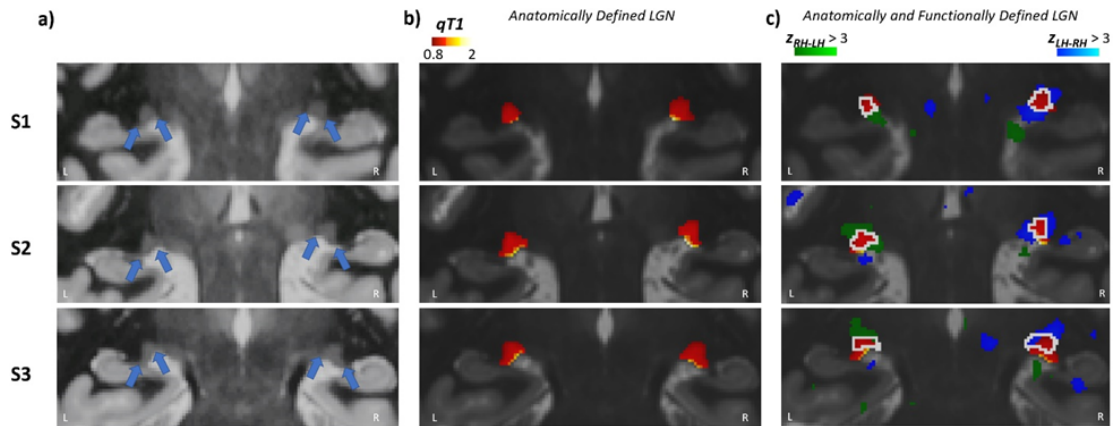
Figure 1.3: Masks for Lateral Geniculate Nucleus (LGN). For each participant in separate rows, a) the average qT1 map of a coronal slice, contrast and brightness of the images were adjusted for this illustration, b) the color-coded qT1 maps within each LGN, c) LGN localizer results showing the significant functional activity for the contralateral visual hemifield compared to the ipsilateral hemifield (LH: left hemifield, RH: right hemifield), which is used to adjust the LGN masks for visual activity (white outline).

1.3.2 M and P Layer Segmentation with qMRI

The qT1 results for the M and P subdivisions were anatomically reliable. First, as can be seen in the histograms in Figure 1.4a, the P voxels had shorter T1 relaxation than the M voxels, $p < .001$ for all LGN, suggesting more myelination in the P layers. This result is in line with Müller-Axt et al.'s (2021) who also found shorter qT1 for the P segment using a 7T scanner, pointing out more myelination in the P compared to the M segment. Also, as can be seen in Figures 1.3b and 1.4b, there was a gradient change in qT1 activity from P to M layers. P voxels that had a qT1 value closer to the threshold (dashed line in Figure 1.4a) were also spatially closer to the M set. This gradient nature of qT1 map within LGN was consistent across all slices for all subjects. More importantly, the M and P subdivisions spatially complied with the anatomical locations. As evident in Figure 1.4b, the M voxels occupied the

ventromedial layers while the P voxels occupied the dorsolateral layers of LGN for all subjects. Last, the identified M voxels made up 11.7%, 15.8%, and 16.0% of the left LGN and 18.9%, 17.0%, and 16.6% of the right LGN for each subject respectively. These proportions are similar to what had been reported in histology studies (Andrews et al., 1997; Selemon & Begovic′, 2007). All these results suggest that the M and P segmentation based on the qT1 values in LGN is anatomically consistent in their proportions, myelinations, and spatial locations within LGN.
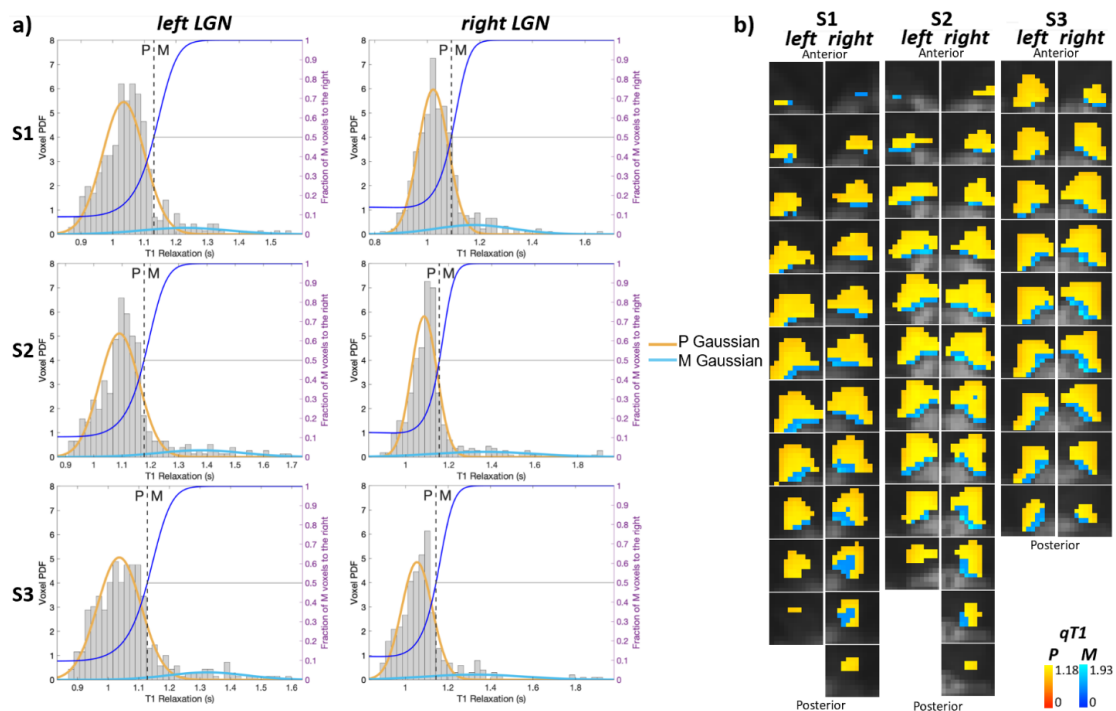
Figure 1.4:   qMRI Results for Each Participant. a) Histograms of voxels for each LGN. The x-axis is the qT1 values, the left y-axis is the voxel probability density function, and the right y-axis is the fraction of M voxels to the right of the distribution for a given cut-off value which is plotted with the dark blue line. Yellow and blue lines show the Gaussian fits for M and P resulting from a two-component mixture model of the data, as detailed in Section 2.2.2.1. b) qT1 maps color-coded within the M and P, separated based on the cut-off indicated by the dashed line in a.

1.3.3 Eye-specific Layer Segmentation with fMRI

The results of the monocular and dichoptic tasks, as well as a statistical combination of the two tasks, are shown in Figure 1.5. Figure 1.5a color codes the voxels as responding to the contralateral (cool colors) and ipsilateral (warm colors) stimuli for each LGN, when calculated based on the sign of the t-score for LE vs RE contrast. Figure 1.5b shows only the voxels that exhibited a significantly different response between the eyes. The monocular task resulted in a stronger ocular preference compared to the dichoptic task. This result can be seen in Figure 1.5a in the combined results for the two tasks (third row for each subject) which appeared more similar to the monocular condition for each particular subject (first row). Accordingly, the dichoptic task significantly activated fewer voxels (Figure 1.5b). Thus, the eye signals were stronger in LGN when the other eye was closed instead of being open and presented with a blank screen. The contribution from the non-stimulated eye on the signals for the stimulated eye differed between tasks.

There was a RE dominance evident in both tasks, as seen in Figure 1.5a and 1.5b, there were more ipsilateral voxels in the right LGN (red) while more contralateral voxels were identified for the left LGN (blue). Also, the RE bias is evident in Figure 1.5c, which shows the scatterplots of the t-scores of each voxel for RE and LE conditions separately. The black lines in Figure 1.5c indicate equal t-scores, i.e., no ocular preference. Thus, the more numerous voxels that fall above the black line were classified as RE and the fewer voxels below as LE. The exceptions to this RE bias were observed in the monocular task in S1's left LGN, which had more voxels preferring the LE, and in S3's left LGN, which had equal number of RE and LE voxels. On average, the percentage of RE voxels to the LGN was 56.5% for the

left LGN and 65% for the right LGN with the dichoptic task whereas it was 44.5% for the left LGN and 64.3% for the right LGN with the monocular task.
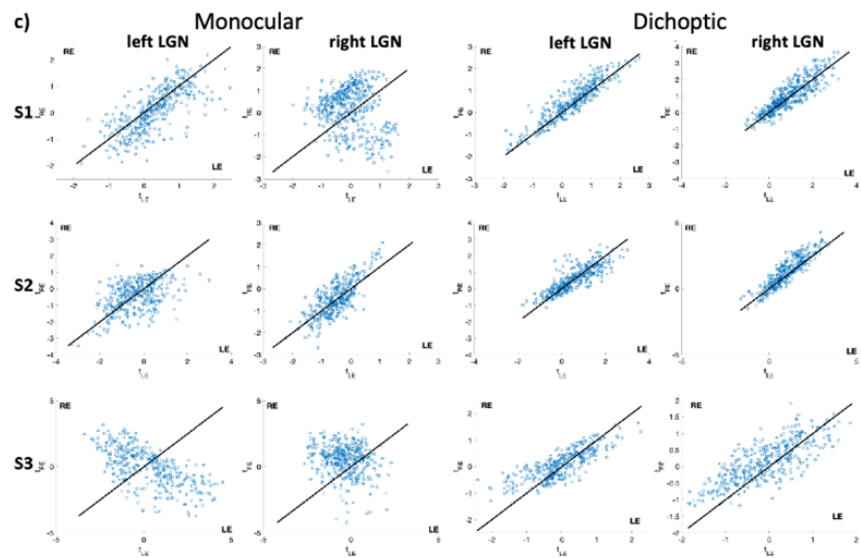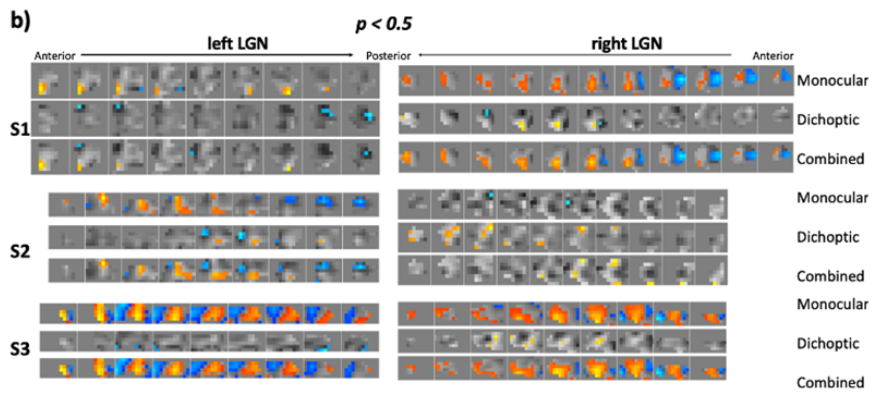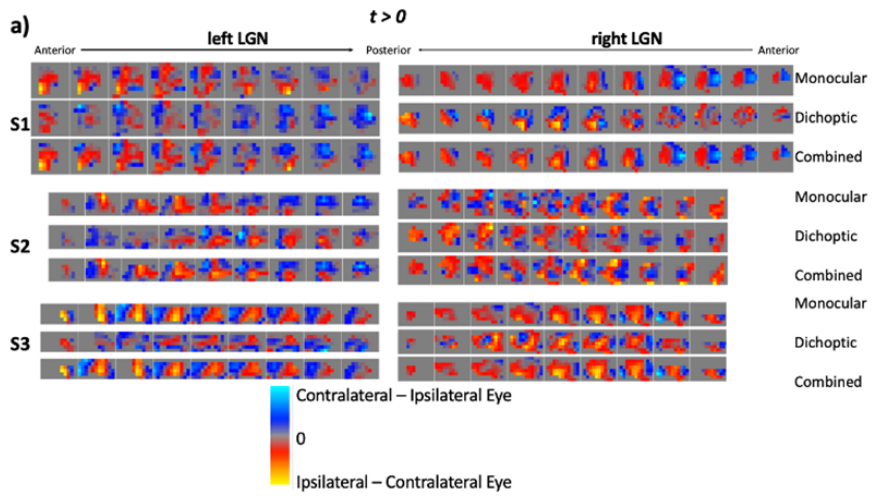
Figure 1.5:   Eye-specific Activity for Each Participant. For the monocular eye
              localizer, participants closed one eye at a time. For the dichoptic eye
              localizer, one eye was shown with blank while the other eye was visually
              stimulated. a) The ocular preference was calculated based on the t values
              for Left Eye – Right Eye in the eye localizer analysis. b) The voxels
              showing significant ocular preference for Left Eye – Right Eye contrast.
              c) Scatterplots of the t values for Left Eye (x-axis) and Right Eye (y-axis)
              for each task. The black lines are the lines of equality indicating no
              ocular preference for the voxel.

Figure 1.6 displays the correlations for each voxel between the ocular preferences with different tasks, i.e., t-score for LE – RE. The correlation between the tasks was significant for five out of six LGN, p's ≤ .001. All the significant correlations increased when we used only the voxels that were significant in their ocular preference in the combined analysis of the two tasks (the third row for each subject in Figure 1.5b), as indicated by the red dots and the corresponding red line in Figure 1.6. The LGN that did not show significant correlation (S2 right LGN) also failed to show significant voxels.
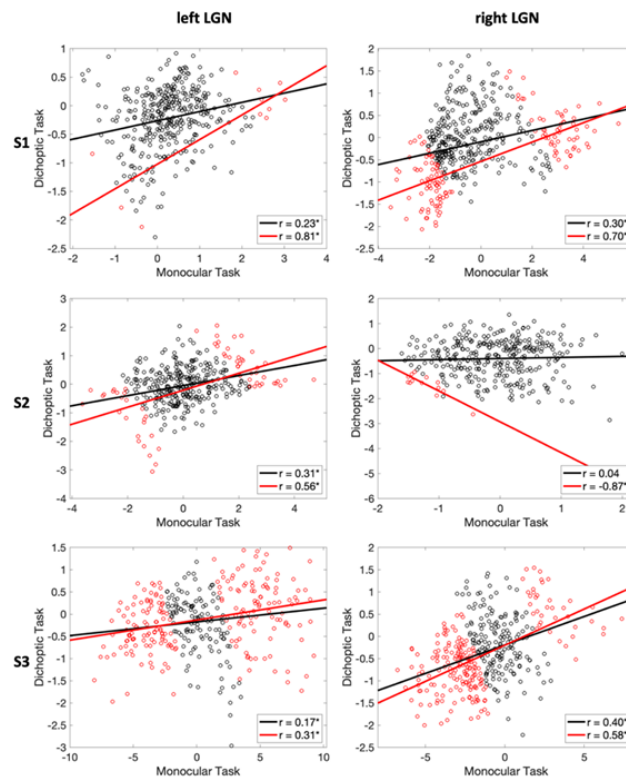
Figure 1.6: Scatterplots of Voxels' Ocular Preference with the Eye Localizer Tasks. The red dots are the voxels whose ocular preference was significant in the combined analysis of the monocular and the dichoptic tasks. The solid lines show the correlation between the two tasks (black for all voxels and red for only the significant voxels. *$p \leq .002$

To test the significance of the LE vs RE classification, based only on the sign of their t-scores and ignoring the magnitude, we conducted a chi-square analysis for each LGN on the resulting categorical variables (Table 3.1). The classification of the voxels matched between the two eye localizer tasks on only four of the six LGN, p's < .001. These significant results were driven by the RE bias in the classification. A close inspection of the cross-tables in Table 1.1 indicated that there was more match between the RE voxels (the upper left cell for each subject's each LGN) than between the LE voxels (the lower right cell) for the majority of the LGN.

Table 1.1: Chi-square results for Left Eye (LE) and Right Eye (RE) categorization

| | | | *Number of voxels* | | | | χ^2 | | p | |
			left LGN		**right LGN**		**left LGN**	**right LGN**	**left LGN**	**right LGN**
			Dichoptic Task							
			RE	*LE*	*RE*	*LE*				
S1		*RE*	87	31	205	93	11.3	27.7	**< .001**	**< .001**
		LE	138	111	65	86				
S2	*Monocular Task*	*RE*	115	72	123	56	14.1	2.24	**< .001**	.13
		LE	74	103	95	61				
S3		*RE*	100	70	218	60	.97	37	.33	**< .001**
		LE	91	79	47	55				

Table 1.2 shows the chi-square results for the voxels showing significant ocular preference in the combined analysis of the two tasks. The RE bias was reduced

when only the significant voxels were classified and the classification with the two

tasks significantly matched again for four out of six LGN, p's < .001.

Table 1.2: Chi-square results for Left Eye (LE) and Right Eye (RE) categorization for only the voxels that showed significant ocular preference in the combined GLM analysis.

		Number of voxels				χ^2		p	
		left LGN		**right LGN**		**left LGN**	**right LGN**	**left LGN**	**right LGN**
	Dichoptic Task								
		RE	*LE*	*RE*	*LE*				
S1		*RE* 3	0	78	1	3.44	61.52	.064	**< .001**
		LE 3	5	22	35				
S2	*Monocular Task*	*RE* 25	0	13	-	48.59	-	**< .001**	-
		LE 4	34	-	-				
S3		*RE* 73	32	152	12	18.95	118.41	**< .001**	**< .001**
		LE 91	79	47	55				

My goal in identifying the eye-specific layers was to segment the M and P

layers. I tried to identify the contralateral layers positioned most ventrally or dorsally

to find the contralateral M or P regions, respectively. The dorsal contralateral layer

appeared robustly with either eye localizer task for all LGN using the signed

classification (Figure 1.5a), and in four of six LGN using only the voxels activated

significantly by the combination of both tasks (Figure 1.5b). However, the ventral

contralateral layer did not appear reliably. The ventral contralateral layer could be

identified in only two LGN in one or other of the tasks (Figure 1.5a), though the

successful task differed between the two LGN (monocular task for S1 left LGN and dichoptic task for S3 left LGN). Using only the significant voxels in the combined analysis (Figure 1.5b, third row for each subject), the ventral contralateral layer can only be identified for S3. Instead of reliable individual layers, we could identify a contralateral eye cluster located more dorsolateral and an ipsilateral eye cluster located more medioventral (Figure 1.5b).

1.4   Discussion

To segregate the M and P regions in human LGN, I used MRI methods that were not dependent on the stimulus characteristics, unlike the previous attempts (Denison et al., 2014; Zhang et al., 2015) that were confounded by the stronger activation of hilum of LGN (DeSimone & Schneider, 2019). Using qT1 (i.e., measuring the T1 relaxation time for each voxel), I successfully identified the M and P components of both LGN in all the subjects, which conformed to our anatomical expectations. However, attempting to identify the individual ipsi- or contralateral layers using fMRI was less successful. The identification of eye layers was more consistent with the monocular task than the dichoptic task. The P layers in the dorsal contralateral cluster could be readily identified, but the ventral contralateral layer was not consistently activated.

qMRI, with a MP2RAGE sequence we used, has been shown to be more advantageous for subcortical structures. Aldusary et al. (2019) compared different T1 sequences for LGN volume and found that MPRAGE imaging was more accurate compared to proton density imaging with a 3T scanner. Using the MP2RAGE sequence with two inversion times allowed me to calculate the T1 parameter for each voxel, which enhanced the segmentation of the whole LGN relative to an MPRAGE or

proton-density weighted sequence and also allowed the segmentation of the M and P divisions. The whole LGN volumes I found were consistent with post-mortem histology (Andrews et al., 1997) and with the structural MRI studies with a 3T scanner (proton density imaging in Giraldo-Chica et al., 2015; phase difference enhanced imaging in Kitajima et al., 2015; T1-weighted imaging in Wang et al., 2015). On the other hand, when defined functionally, previous studies reported much higher volumes of LGN (Denison et al., 2014; Kastner et al., 2004), likely as a result from the difficulty of segmenting the LGN from surrounding visually active regions such as the lateral and medial pulvinar.

To segregate the M and P regions based on the qT1 maps, I followed a data-driven approach. By fitting a two-component model to the qT1 data, the smaller proportion component was selected as M and the larger proportion component as P. The P component showed shorter T1 relaxation time (i.e., qT1) than the M component, indicating more myelination in the P layers. This is consistent with the other qMRI studies (Müller-Axt et al., 2021; Oishi et al., 2020) and with higher cell density and more myelination in the P compared to the M divisions (Hassler, 1966; Pistorio et al., 2006). Previous studies used a fixed proportion as the criterion to segregate the M and P sections (Denison et al., 2014; Oishi et al., 2020), based on the histology findings that, on average, 20% of the LGN is M (Andrews et al., 1997; Selemon & Begovic´, 2007), but this approach, even if correct, would not allow the independent measurement of the M division properties. Individuals show great variation in the proportions of the subdivisions (Andrews et al., 1997; Müller-Axt et al., 2021), and indeed the participants in the current study had M divisions ranging from 12–19% of the LGN volume.

My investigation of the eye dominance signals did not yield consistent results with the monocular vs. dichoptic eye localizer tasks. The eye-specific signals were higher in amplitude with the monocular task than with the dichoptic task such that it was difficult to measure significant activation with the dichoptic task despite the same amount of data. This might indicate higher interference from the "non-stimulated" eye in the dichoptic presentation set-up. However, both tasks resulted in a right eye dominance in LGN, consisting of 57.6% of the LGN volume on average. The classification of the RE voxels was more consistent between the tasks than for the LE voxels. Previous studies identifying the eye preference of the voxels did not measure layer-like organization, nor did they compare different tasks (Haynes et al., 2005; Qian et al., 2020). I found that the dorsal contralateral layer, classified as P, could be reliably identified with both monocular and dichoptic tasks, whereas the ventral contralateral layer, which would be classified as M, could not be reliably activated with either task. Critically for the fMRI methods, the hilum region of LGN did not dominate the responses to eye-specific stimuli when the other eye was closed. However, the right eye bias did interfere with the ability to classify the eye-specific layers, and functionally identifying the eye-specific layers does not appear to be a promising approach to segmenting the M and P regions of the LGN.

1.4.1 Conclusion

The qT1 results in this study replicated Müller-Axt et al. (2021) using a 3T scanner. Moreover, I found consistent qT1 results within and between individual participants, whereas Müller-Axt et al. (2021) only showed group results. This is perhaps due to the much larger volume of data at 7T and due to their aim in creating an atlas in a standard space. Overall, my results demonstrate that the qMRI methods

are promising in finding LGN as well as in separating its M and P subdivisions while the functional identification of contralateral layers of M and P remains challenging.

Chapter 2

COMPUTATIONAL ANALYSIS OF EYE-SPECIFIC SIGNALS IN HUMAN LATERAL GENICULATE NUCLEUS

2.1　Introduction

The availability of high refresh rate projectors allows their use in the functional magnetic resonance imaging (fMRI) design to present stereoscopic stimuli. This can be used to stimulate each eye separately and therefore valuable for vision research. For example, lateral geniculate nucleus (LGN), the relay station in the thalamus in visual processing, is composed of neurons receiving input from one eye only. The contralateral eye neurons and the ipsilateral eye neurons are both present in the LGN but organized in a layered structure (see Figure 1.1a). Identifying the eye-specific structure can be useful to understand the function of the LGN, as indicated for visual phenomena such as binocular rivalry (Haynes et al., 2005; also see Chapter 3) and for visual development impairments such as amblyopia (Hess et al., 2009).

In Chapter 1, I aimed at separating the eye-specific layers in the lateral geniculate nucleus (LGN) with functional magnetic resonance imaging (fMRI). However, how the participants viewed the monocular visual stimulus mattered. The eye-specific structure in the LGN was not as consistent when the participants closed each eye alternately (i.e., monocular viewing) and when they kept their eyes open, but a blank screen and a stimulus was presented to each eye alternately (i.e., dichoptic viewing). This poses a problem because there has been research using these viewing conditions separately to identify the eye-specific regions in the LGN (Haynes et al.,

2005; Qian et al., 2020). My goal, in this chapter, was to test the same data to see if similar eye-specific structures in the LGN can be achieved with the two different viewing conditions.

In previous research (Haynes et al., 2005; Qian et al., 2020) and in Chapter 1, the eye-specific data were analyzed with a generalized linear model (GLM) that contrasted the activity for the times of left eye (LE) vs right eye (RE) stimulation. The ocular preference of the voxels was determined based on the sign of the t-score for LE–RE contrast, positive scores indicating a LE preference and negative scores indicating a RE preference. However, my investigation in Chapter 1 revealed that the monocular viewing results in stronger signal than the dichoptic viewing as suggested by the combined GLM for the two viewing conditions. Therefore, I sought for an alternative analysis to find the eye-specific structure in the LGN that were more reliable across the viewing conditions, when analyzed separately. Specifically, I utilized from an unsupervised method that captures the inherent structure in the data, without the need of specifying the LE and RE stimulation times unlike in GLM.

2.1.1 Orthonormal Projective Non-negative Matrix Factorization (OPNMF)

Non-negative matrix factorization (NMF) refers to an unsupervised technique that finds the inherent components that describe a non-negative data matrix (D. Lee & Seung, 2000). NMF is similar to other more commonly used unsupervised techniques, such as principal component analysis (PCA; Shlens, 2014a) and independent component analysis (ICA; Shlens, 2014b), in that all these methods approximate the data with a lower number of components based on the multivariate relations. Parts of the data are associated to different components in proportion to the associated coefficients. The main difference between NMF and the other methods is that the

25

NMF estimates for the components are non-negative: the coefficients can be zero, meaning that the particular part of the data does not belong to the component, or they can be positive, indicating the intensity at which the particular part of the data belongs to the component.

Generally, NMF requires estimating both the coefficients and the components. An alternative is to use projective NMF (PNMF), which estimates only the components—the coefficients are the result of projecting the data onto the components (Yang & Oja, 2010). Here, I used the PNMF with the orthonormality constraint (OPNMF) which resembles to PCA such that the components are restricted to be orthonormal. Together with non-negativity, the orthogonality constraint ensures that the components are each sparse, providing an interpretable parts-based approximation. Like PCA, OPNMF attempts to minimize the sum of squared errors between the data and the component-based approximation. However, unlike PCA finding the optimal components is not guaranteed. Thus, the main benefit of OPNMF over PCA is that its estimates of the non-negative components are more interpretable (Sotiras et al., 2015; Türkmen, 2015).

OPNMF has been used in the MRI research with the structural and diffusion tensor imaging data to find the covarying brain structures (e.g., Sotiras et al., 2015). It has been also demonstrated to be useful in identifying the microstructures in brain regions like hippocampus (R. Patel et al., 2020) or striatum (Robert et al., 2022). However, no study to date has employed OPNMF analysis on the fMRI data. Thus, this study also aimed to show the first use of OPNMF on a high dimensional event-related functional data to identify a structure within a brain region.

2.2 Methods

2.2.1 Data

The data was what was obtained in Chapter 1 with the monocular and dichoptic eye localizers (see Section 1.2.2.3 for details). Separately for the three participants, the pre-processed time-series data (see Section 1.2.2.3.4) from each eye localizer scan was aligned to the participant's native space (see Section 1.2.2.1) and masked for their left and right LGN (see Figure 1.3c). The first 6 s (i.e., 4 volumes) of each scan and the motion outlier volumes (see Section 1.2.2.3.4) were discarded. Then, the time series data from each scan were concatenated for the monocular and the dichoptic eye localizer tasks separately as well as in a combined fashion by concatenating their data, resulting in three datasets for each six LGN. The volumetric image was vectorized for each LGN so that the datasets included a $D{\times}N$ matrix where D was the number of voxels and N was the number of time samples.

2.2.2 OPNMF analysis

The datasets were analyzed in MATLAB using opnmf_mem.m code available at https://github.com/asotiras/brainparts. This code was developed by Sotiras et al. (2015), based on the original OPNMF described by (Yang & Oja, 2010), for the approximation of high-dimensional imaging data with K number of components. To alleviate the cost associated with the high dimensionality, the multiplicative update rule was modified by Sotiras et al. (2015), ensuring non-negative estimates while decreasing the energy to reach an optimum, by adopting a Non-Negative Double Singular Value Decomposition initialization strategy (Boutsidis & Gallopoulos, 2008). There could be maximum 50000 iterations until the convergence factor of $1{\times}10^{-5}$ was

reached. The non-negative estimates for each component were W, the weights for each voxel, and H, the coefficients for each time sample.

First, OPNMF was employed on the data with the number of components, K, set to two which could account for the eye-specific signal and noise. For each voxel in the LGN, I took the difference between the estimated weights associated with each component. Since the estimates were non-negative, this calculation indicated the relative weight of the voxel in reflecting one component. However, it was also possible that the signals would be captured separately for each eye; therefore, I also employed the OPNMF analysis with three components so that the third component might capture the noise. Nevertheless, because OPNMF is an unsupervised method, what function the components would reflect could not be determined beforehand.

2.3   Results

2.3.1   2-component OPNMF

When there were two components ($K = 2$), the OPNMF analysis estimated components that differed in their associated coefficients across all time samples, i.e., $H_1 > H_2$. The component with the higher coefficient was named as K_1 and the other as K_2, and the weights associated with these components can be seen in Figure 2.1a for each LGN. As clearly illustrated in the Figure 2.1a, the results were highly consistent between the two viewing conditions (the first vs the second row for each subject), especially for S1 and S3. The comparison with the GLM results in Figure 1.5a and Figure 1.5b (combined results in the third row for each subject) indicated that K_1 corresponded to dorsally located contralateral eye regions (cool colors) and K_2 corresponded to medially located ipsilateral eye regions (warm colors), for both left

and right LGN. Similar to the GLM results, the contralateral M layer, the most ventral layer in the LGN (see Figure 1.1), was not found with the 2-component OPNMF analysis. Last, the combined data from the two viewing conditions did not resemble to any of these results (the third row vs the first and the second row for each subject in Figure 2.1a), possibly the components included more noise due to the two viewing conditions.
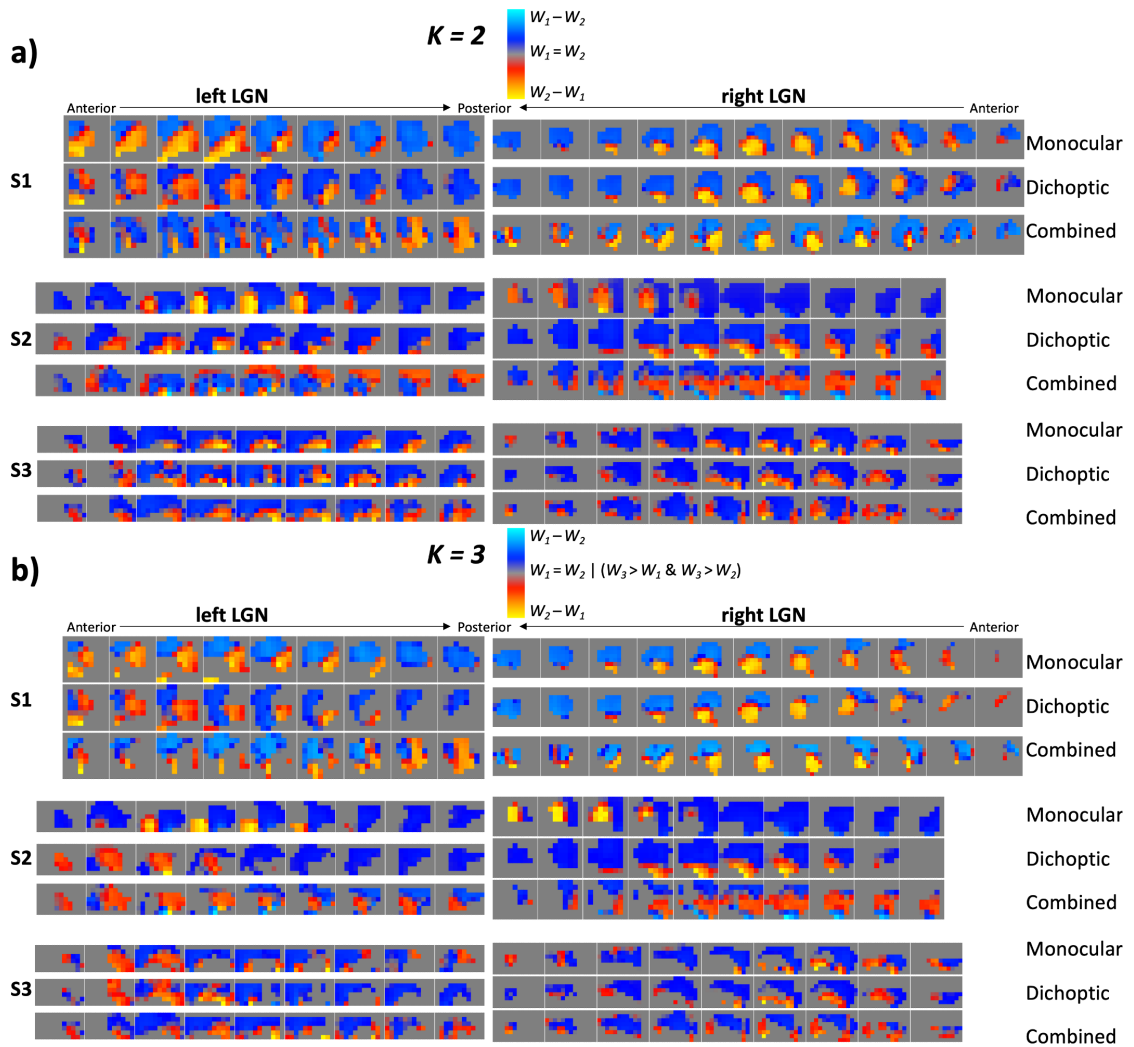
Figure 2.1: OPNMF Results for Each LGN. For the monocular eye localizer, participants closed one eye at a time. For the dichoptic eye localizer, one eye was shown with blank while the other eye was visually stimulated. K: number of components for the OPNMF analysis, a) two components vs b) three components. W_1: estimated weights for the component with the higher overall coefficient, W_2: estimated weights for the component with the lower overall coefficient. W_0: estimated weights for the component with the lowest overall coefficient when there were three components.

I also tested the correspondence between the data from the two viewing conditions in classifying the voxels into two components. Each voxel was categorized as K_1 if W_1 was estimated to be larger than W_2 (cool colored voxels in Figure 2.1) or as K_2 if it was smaller (warm colored voxels). Table 2.1 shows the chi-square results which were significant for all six LGN when the p values were not corrected for multiple comparisons for six LGN (see p's in the table). A close look at the cross-tables for each LGN revealed that there was a significant match between the two conditions in the categorization of voxels (upper left and lower right cells). However, the match was mostly for the K_1 voxels which seemed to be the contralateral eye regions (Figure 2.1a). Still, the OPNMF results were more consistent across the monocular and the dichoptic viewing conditions than the GLM results (Table 2.1 vs Table 1.1).

Table 2.1:   Chi-square results for 2-component categorization (K_1 and K_2)

			Number of voxels				χ^2		p	
			left LGN		right LGN		left LGN	right LGN	left LGN	right LGN
			Dichoptic Task							
			K_1	K_2	K_1	K_2				
S1		K_1	204	17	268	19	166.24	214.16	**< .001**	**< .001**
		K_2	40	106	44	118				
S2	*Monocular Task*	K_1	190	97	182	87	14.38	6.29	**< .001**	**.01**
		K_2	68	9	55	11				
S3		K_1	198	54	231	38	58.42	110.5	**< .001**	**< .001**
		K_2	30	58	35	76				

2.3.2   3-component OPNMF

When the number of components was determined as three ($K = 3$), the OPNMF coefficient estimates were again different for the components across all the time series. One component (K_3) had the lowest coefficient (i.e., H_3 close to zero) while the other two components (K_1 and K_2) had coefficients more similar to each other than to K_0's. Figure 2.1b shows the LGN slices, color coded for the difference in the estimated weights for K_1 and K_2. The gray voxels are those whose estimated weight for K_0 was larger than that for K_1 and K_2, or those who had equal weights for K_1 and K_2. The results in Figure 2.1b were highly consistent between the two viewing conditions (the first two rows for each subject), especially for S1 and S3. Like the 2-component OPNMF, the 3-component OPNMF found eye-specific structures where K_1 corresponded to dorsally located contralateral eye regions (cool colors) and K_2 corresponded to medially located ipsilateral eye regions (warm colors), for both left and right LGN. Similar to the GLM and the 2-component OPNMF results, the contralateral M layer did not appear. Last, even though the combined data of the two viewing conditions did not look as similar to the results with the separate analysis of the conditions (the third row vs the first and the second row for each subject in Figure 2.1b), it lead to better structure estimate when analyzed with the 3-component OPNMF than with the 2-component OPNMF (the third row for each subject in Figure 2.1a vs Figure 2.1b).

I also tested the correspondence between the data from the two viewing conditions in classifying the voxels into three components. Each voxel was tagged as K_3 if the estimated weight for the voxel was the highest for K_3 (majority of the gray colored voxels in Figure 2.1b), as K_1 if it was the highest for K_1 (cool colored voxels),

or as K_2 if it was the highest for K_2 (warm colored voxels). The chi square results were highly significant for all the LGN, p's $< .001$ even when Bonferroni corrected for six tests (see Table 2.2). An inspection of the cross-tables in Table 2.2 indicated that there was a significant match between the two conditions in the categorization of the voxels in each LGN (the diagonal from upper left to lower right). As was the case with the 2-component analysis, the match was mostly for the K_1 voxels (especially see S2); however, the numbers were reduced accounting for the third category of the K_0 voxels (Table 2.1 vs Table 2.2 for the match between K_1).

Table 2.2: Chi-square results for 3-component categorization (K_1 and K_2). * $p < .001$

									Number of voxels	χ^2	
			left LGN			right LGN			left LGN	right LGN
						Dichoptic Task					
			K_1	K_2	K_3	K_1	K_2	K_3		
S1		K_1	116	4	46	170	20	4		
		K_2	1	81	36	8	97	30	195.53*	409.2*
		K_3	54	16	13	17	16	87		
S2	*Monocular Task*	K_1	118	66	73	165	56	34		
		K_2	32	9	13	50	0	0	35.12*	61.02*
		K_3	47	6	0	10	20	0		
S3		K_1	128	18	20	179	25	7		
		K_2	39	50	16	30	49	10	121.27*	263.37*
		K_3	12	18	39	10	12	58		

2.4   Discussion

This study indicated that the OPNMF analysis of the monocular and dichoptic eye localizer data is better at capturing the eye-specific structure in the LGN than the GLM analysis. The GLM results in Chapter 1 were reliable only when the two viewing conditions were combined in a higher-level GLM analysis which accounted for the difference in the signal amplitude between the two conditions. However, the OPNMF results here were highly consistent for the monocular and dichoptic viewing conditions when analyzed separately.

When the data was approximated with 2-component OPNMF, the initial reasoning was that the two components would reflect the eye-specific signal and noise, but it was also possible that one component would reflect one eye's signal while the other component reflects the other eye's. However, the structure in the LGN suggested that the first component captured the contralateral eye signal while the second component captured the ipsilateral eye signal. In Chapter 1, the GLM lead to a RE bias in the LGN structure while the OPNMF here lead to a contralateral eye bias. Because of its orthogonality constraint, the contralateral eye signal (the first component) was stronger for LGN than the ipsilateral eye signal (the second component), indicated by the higher coefficients across the time series for the former. To see if noise could be separated from these two signals, I conducted 3-component OPNMF. Even though the OPNMF estimated more similar coefficients for the two components when a third one was added, the match between the categorization of the voxels still was dominated by the contralateral eye component.

When interpreting the components found in the LGN, it should be noted that the various sources of information could have contributed to the components. For

example, the M and P layers of the LGN might have interfered with the with the eye signals (see Figure 1.1). In fact, this might be driving the lack of the contralateral M layer, with both the GLM and the OPNMF analysis. The contralateral eye signals in the P section might be dominating the structure found in the data, resulting in eye-specific clusters instead of layers. Or the components might have also captured the anatomical differences such as the hilum region in the LGN or the blood vessel next to LGN (Abbie, 1933). The hilum is where the blood vessels enter the LGN from the medial parts. The hilar area has a functional role in the central vision and along the horizontal meridians in the visual field (Abbie, 1933) and exhibits higher amplitude fMRI response to a range of visual stimuli (DeSimone & Schneider, 2019).

This third component in the OPNMF analysis appeared to have captured something other than the monocular eye signals, but it could be the hilar area (e.g., gray voxels for S3 in Figure 2.2) or the blood vessel (e.g., gray voxels for S1 right LGN or S2 left LGN), or the noise associated with respiration, pulse, and other motion during scanning (e.g., gray voxels in between the cool and the warm colored clusters). These findings suggest that OPNMF analysis can be improved with a greater number of components to account for different sources of information in the LGN.

2.4.1 Conclusion

The OPNMF analysis in this study was evidently more advantageous over the GLM in identifying the eye-specific structure in the LGN. I found consistent structures in the LGN with the data from the monocular and the dichoptic viewing conditions. Therefore, this study suggests OPNMF as a more reliable analysis of the eye-specific data in the LGN than what was used previously in the literature (Haynes et al., 2005; Qian et al., 2020). Also, although other variants of NMF have been used to uncover

brain networks indicated by the resting state functional data (e.g., Aggarwal & Gupta, 2018; Li et al., 2018), no study to date has tested NMF on the event-related fMRI data. Here, I revealed that OPNMF is promising in identifying a functional structure in a brain area.

Chapter 3

NEURAL DYNAMICS DURING BINOCULAR RIVALRY: INDICATIONS FROM HUMAN LATERAL GENICULATE NUCLEUS

3.1   Introduction

Our experience of the visual world is a single view even though the visual information is received by the two eyes. For a unified percept, there must be a combination of each eye's output, requiring an interaction between the eyes. For example, we perceive a single object when it is positioned in the same coordinates of the physical world on our retinae with the same form, speed, and direction of motion. In other words, there is correspondence on each eye's retinal map for the spatiotemporal characteristics of the same form, providing the inference for a unified perception of the individual object. Binocular rivalry refers to the failure of a unified perception due to the lack of such correspondence, resulting instead in a rivalrous perception (Blake, 1989).

Binocular rivalry (BR) occurs when each eye is presented with a sufficiently different stimulus, resulting in a competition of these monocular stimuli for perception (Alais & Blake, 2015). It is an interesting phenomenon in that BR sets an example where visual consciousness fails to capture reality. Even though there are two pieces of visual information in the physical world, we cannot perceive them at the same time; instead, perception alternates between these stimuli. Thus, BR provides a mean to study the correlates of visual awareness in the brain (Blake et al., 2014; Rees, 2009; Tong, 2003); specifically, the correlates of the resolution of visual competition.

Figure 3.1 shows an example BR paradigm where the right eye is presented with a car image while the left eye with a house image using mirror stereoscope. These non-matching stimuli in the retinal position of the two eyes create a conflict because a location in the world cannot be occupied by a house and a car at the same time. To resolve this conflict, our perception typically alternates between these two stimuli. While one stimulus dominates the perception and is visible to consciousness, the other stimulus is being suppressed and consciously invisible. This goes back and forth between the two images at irregular intervals, as illustrated by an example participant response in the bottom part of Figure 3.1. However, if the stimuli are not matched evenly in terms of low-level features, or if they are too large or more ambiguous (e.g., low-contrast, low spatial frequency), then piecemeal rivalry or fusion occurs more often where perception is a mixture of both images in parts.

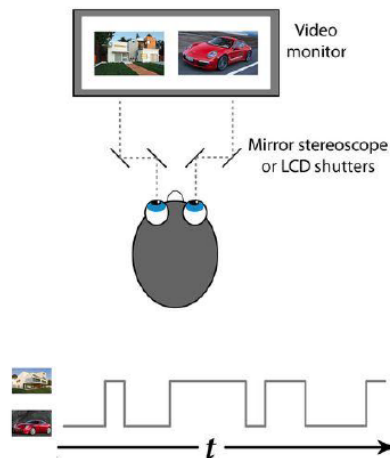Figure 3.1:   Example Binocular Rivalry. The top part shows the monocular presentation of each image. The bottom part shows the fluctuation in perception across two monocular images irregularly over time (t). Adapted from "Binocular Rivalry and Perceptual Ambiguity" by D. Alais and R. Blake (2015) in J. Wagemans (Ed.), Oxford Handbook of Perceptual Organization, New York: Oxford University Press.

In this study, I aimed to investigate the neural mechanisms of BR, focusing on the two parallel streams of visual processing, i.e., magnocellular (M) and parvocellular (P) pathways, and their contribution to the resolution of competition, and thus to visual awareness, during binocular rivalry. Using magnetic resonance imaging (MRI), I examined the lateral geniculate nucleus (LGN), a part of thalamus in the brain that M and P neurons are disjoint in its layered structure (see Chapter 1 for details on LGN structure and its M and P parts).

3.1.1 Neural Mechanisms of Binocular Rivalry

The literature on the neural mechanisms of BR evolved around the question of whether the visual competition is resolved at sensory-level or higher-levels in the visual processing hierarchy. These views emerged from the debate between eye rivalry vs stimulus rivalry (e.g., Lee & Blake, 1999; Leopold & Logothetis, 1999). In the BR paradigm, it is not certain what is competing for visual awareness. The house and the car in Figure 3.1 are objects so that we might think that it is the stimulus representations that are competing, i.e., stimulus rivalry. Nevertheless, these stimuli are viewed by different eyes. Therefore, we can also think that it is the monocular representations that are competing, i.e., eye rivalry.

A direct investigation of the stimulus vs eye rivalry was done by Blake and his colleagues (1980) by eliminating the correspondence between the stimulus and the eye with an eye-swapping procedure. They presented a horizontal grating to one eye and a vertical grating to the other eye. Participants' task was to press and hold a key when they exclusively perceive the vertical grating and release it when they start to see the horizontal grating. In the critical reversal condition, the gratings were shut off for 4 ms upon the participant's report of exclusive dominance and then reappeared in the

opposite location. In other words, the gratings were swapped between the eyes, resulting in the dominant grating being presented to the eye that was "seeing" the suppressed grating and the suppressed grating being presented to the eye that was "seeing" the dominant grating. Importantly, this reversal condition resulted in a switch in the dominant stimulus. After the eye-swap, the view of the eye that was already dominant remained dominant which led to the perceptual report of the previously suppressed stimulus. This and other early behavioral studies (e.g., Blake & Fox, 1974; Fox & Check, 1966; Wade & Wenderoth, 1978; Wales & Fox, 1970) indicated that the competition was between each eye's view, i.e., interocular competition or interocular conflict, rather than between the presented stimuli.

Corresponding to the eye rivalry idea, advocates of the sensory-level explanations posit a critical role for mutual inhibition between the monocular neurons (Blake, 1989; Lehky, 1988; Tong, 2001; Wolfe, 1986), neurons that receive input from either the left eye or the right eye exclusively. All the neurons in LGN and some neurons in V1 receive such monocular input. Therefore, suggested models focus on these areas as the resolution site of conflict. In support for this, human studies demonstrated that V1 activity is highly correlated with the perception during BR (Haynes & Rees, 2005; S. H. Lee et al., 2005; Parkkonen et al., 2008; Polonsky et al., 2000). Since V1 is composed of both monocular and binocular neurons, these studies do not give direct support for the monocular explanations of BR (but see Tong & Engel, 2001).

LGN, however, is composed of monocular neurons only (see Chapter 1 for details). Two human studies found strong correlations between LGN activity and their participants' percept during BR (Haynes et al., 2005; Wunderlich et al., 2005). Haynes

et al. (2005) showed that the dominant eye during rivalry was reflected in the fMRI activity in the LGN's eye-specific regions. In addition, Wunderlich et al. (2005) demonstrated that fMRI activity in the LGN reflected the percept of the subject such that perceiving a high contrast grating increased the activity while perceiving a low-contrast grating decreased it. Also, these activity dynamics were the same as when there were physical stimulus alternations without rivalry, indicating a fully resolved perception in LGN. However, the rivaling stimuli in these studies were colored gratings presented to either eye with no counterbalancing across eyes. Haynes et al. (2005) used red and blue orthogonal gratings, both rotating clockwise and were viewed through red/blue filtered glasses. Wunderlich et al. (2005) used red and green orthogonal gratings viewed through red/green filtered glasses. Color might be an important information for LGN; for example, red/green stimuli can be coded by a single channel through red/green opponent neurons. Thus, the suppressed and the dominant stimulus during BR can be represented by the same neurons. One aim of the current research was to extend these studies by investigating whether the eye-specific layers of LGN are correlated with the perception when the rivaling stimuli is not colored and not processed by a single channel.

Corresponding to the stimulus rivalry idea, advocates of the higher-level explanations posit that it is the perceptual organization of the binocular display that has a crucial role in the resolution of rivalry, thus the stimulus representations in the extrastriate areas (further than V1), and this organization is switched by the regions that are primarily related to planning and attention along the frontoparietal network (Leopold & Logothetis, 1999; Logothetis et al., 1996). Mainly, psychophysical observations revealing the importance of stimuli coherence (Alais et al., 2000; Diaz-

41

Caneja, 1928; Jiang et al., 2006, 2007; Kovács et al., 1996; Zhou et al., 2010) and attention (Brascamp & Blake, 2012; Dieter et al., 2016; Ooi & He, 1999; Zhang et al., 2011) gave rise to these explanations. One of the most influential findings supporting stimulus rivalry was observed by Logothetis et al. (1996). They used an eye-swapping procedure with which the stimuli, the two orthogonal gratings, were swapped between the two eyes three times in a second. To mask this swap, the stimuli also flickered at 18 Hz. Participants reported long durations of a dominant stimulus with this interocular switch (IOS) paradigm, similar to their reports with the conventional BR paradigm. A number of analyses further revealed that the characteristics of the perceptual alternations between the two gratings were similar with both paradigms. The slow perceptual alternations between the stimuli, even if they were continually swapping across eyes, indicated that what was dominant or suppressed during BR was the stimulus representations but not what the eye was presented with. Similar results with the IOS paradigm were demonstrated in the literature by other studies as well (Bhardwaj et al., 2008; Bhardwaj & O'Shea, 2012; Denison & Silver, 2012; V. Patel et al., 2015). However, the IOS paradigm does not solely result in slow perceptual alternations. Depending on the spatiotemporal characteristics of the stimuli, participants still report fast alternations as following the swaps between the eyes, indicating an eye level rivalry (e.g., Denison & Silver, 2012; Lee & Blake, 1999; Silver & Logothetis, 2007).

This debate between eye vs stimulus rivalry is old and focused on where the neural site for rivalry is in the visual processing. This assumes a common mechanism for stimulus and eye rivalry (Andrews & Purves, 1997; Logothetis et al., 1996). However, the debate settled around hybrid models (Blake & Logothetis, 2002;

Freeman, 2005; Wilson, 2003; for a review see Tong et al., 2006), as there were evidence favoring both explanations in the brain depending on the stimuli and the paradigm. Hybrid models acknowledge the involvement of different regions along the neural hierarchy to play a role in the resolution of rivalry and propose that the type of stimuli or the way they are presented makes the difference in the recruitment of different brain regions. There is still mutual inhibition between monocular neurons, but there is also mutual inhibition between binocular neurons as well as mutual excitation and feedback connections from frontoparietal regions. These stages may not all be needed. For instance, interocular conflict between simple gratings in a conventional BR paradigm can be resolved at the monocular inhibition stage. However, when the suppression is not complete at the monocular level, such as with the fast flickering and eye-swapping stimulus in the IOS paradigm, the signal can be carried to the pattern selective binocular neurons that are present across multiple levels of visual hierarchy. In other words, the partial suppression of one eye's input escapes the interocular competition at the monocular level, resulting in the competition between binocular neurons representing the swapping stimuli (e.g., Wilson, 2003). Consequently, the mutual inhibition is now between the patterns of stimuli represented by binocular neurons but not between the eyes' view. In this debate of eye vs stimulus rivalry, the fact that the visual system operates in parallel streams, M and P pathways, has been disregarded (He et al., 2005).

3.1.1.1 Binocular Rivalry and the Two Visual Pathways

The two pathways in the visual system raises the possibility that different pathways may contribute differently to the resolution of perceptual competition during BR (He et al., 2005). BR is claimed to be a P pathway phenomenon based on

psychophysical observations (Carlson & He, 2000; He et al., 2005). The stimuli primarily processed by the P pathway result in stronger rivalry than the stimuli primarily processed by the M pathway. Stronger rivalry refers to more complete suppression as indicated by fewer number of perceptual alternations or less piecemeal rivalry. For example, high contrast stimuli (P-stimuli) are better rivaling stimuli with longer times of dominant perceptions (e.g., Levelt, 1965, 1967) while low contrast stimuli (M-stimuli) result in an interocular integration such as dichoptic plaid perception instead of rivalry (e.g., Burke et al., 1999). Or, when the stimuli differ in form or color which are associated with P pathway, they tend to rival but when they differ in temporal frequency which the M pathway is more sensitive to, they tend to fuse into each other (Carlson & He, 2000; O'Shea & Blake, 1986). However, no biases were observed from any pathways regarding spatial frequency with the BR paradigm (for review see He et al., 2005). Note that not all these studies had the aim to explore the two visual pathways and the hypothesis of BR as a P phenomenon.

More direct investigation of the two pathways was carried by Denison and Silver (2012) to explain the mechanisms for eye and stimulus rivalry. They used the IOS rivalry paradigm where the two flickering orthogonal gratings were swapped across eyes in every 1/3 seconds. They compared rivaling stimuli at different flicker frequencies in how much they resulted in slow irregular alternations in perception, i.e., stimulus rivalry, vs fast regular alternations, i.e., eye rivalry. It is previously demonstrated that the stimuli flickering at a higher rate leads to more stimulus rivalry (S. H. Lee & Blake, 1999; Logothetis et al., 1996). In the first experiment, Denison and Silver (2012) observed this result for the gratings with higher spatial frequency (P); however, the gratings with lower spatial frequency (M) showed the opposite. In

their second experiment, they compared rivalry between red/green isoluminant gratings with rivalry between monochromatic gratings. Overall, participants experienced more stimulus rivalry with isoluminant stimuli (P) than monochromatic stimuli (M). In the third experiment, they introduced another condition where the stimuli did not flicker but had a short blank period, immediately before the swap between the eyes. The duration of the blank period was matched with the period of the different flicker rates; the higher frequencies corresponded to shorter blank periods and the lower frequencies corresponded to longer blank periods. The results showed that the higher flicker frequencies and the shorter blank periods decreased the amount of stimulus rivalry between low spatial frequency gratings (M) whereas high spatial frequency gratings (P) were not influenced from these manipulations. These findings indicated that the P-preferred stimuli integrates better to build coherent stimulus representations compared to the M-preferred stimuli in the IOS paradigm. In other words, the fast alternating eye rivalry in the IOS paradigm is associated with the M pathway while slow alternating stimulus rivalry is associated with the P pathway. The conclusion of Denison and Silver (2012) is consistent with slow sustained processing in the P pathway and fast transient processing in the M pathway, and with the conclusion that the exclusive perceptions during rivalry can be attained better with P stimuli than M stimuli (He et al., 2005). Nevertheless, no study to date has tested the M and P pathways involvement in the brain for visual resolution during rivalry.

3.1.2 The Present Research

The goal of this research was to provide a more direct test of the two hypotheses: 1) more contribution of the P pathway to the conventional BR and 2) to the slow alternations in the IOS rivalry. I conducted both the conventional BR

paradigm and the IOS paradigm with the same participants and rivaling stimuli, two identical achromatic gratings rotating in the opposite directions. Brain activity was measured using fMRI while the participants continuously reported which rotation they perceived at the time; clockwise, anticlockwise, or a mixture. To investigate the contribution of M and P pathways to visual resolution during rivalry, I aimed to take advantage of the disjoint M and P layers in the LGN, as identified in Chapter 1.

Another goal was to replicate the results of Haynes et al. (2005) who found that the eye-specific regions of LGN reflected the perceived eye during rivalry. Importantly, by using the achromatic gratings as the rivaling stimuli, I eliminated the color confound that was present in their study. Also, they did not have a control condition in their design for rivalry whereas I included a replay control condition to compare the responses of eye-specific regions to the perceptual alternations induced by the rivaling stimuli vs by the physically alternating stimuli.

3.2 Methods

3.2.1 Participants

The participants for this study were the same as in Chapter 1 (see Section 1.2.1). Relevant to this part of the study, the participants were asked to apply the generic sighting tests to themselves and report their dominant eye. S1 and S2 reported right eye dominance in sighting while S3 reported left eye dominance.

3.2.2 fMRI Procedures and Processing

Each participant was scanned on three different days for maximum 90 min each day. T1-weighted image of each participant was acquired at the beginning of each session, with the same sequence described in Section 1.2.2.1. The T1-weighted

image of each subject from their first session was used to align all subsequent scans which were analyzed in this native space of each subject. The fMRI data were acquired with the same sequence as detailed in Section 1.2.2.3.

3.2.2.1 Binocular Rivalry Experiments

For the dichoptic viewing of the stimuli, the same apparatus for the dichoptic presentation in Chapter 1 was used in this study (see Section 1.2.2.3.3 for details). Participants held a response box on their right hand, their index and middle fingers located on the two buttons. In a session, there were approximately ten 5-minute fMRI scans. During these 5-minute blocks, the participant was instructed to fixate on the central dot in the display, around which they were shown with a rotating grating. They continuously reported the rotation they perceive using the response box. They pressed and held at least one of the two buttons: the button under their right index finger to indicate counterclockwise rotation, the button under their right middle finger to indicate clockwise rotation, or they pressed both buttons at the same time for their mixture perception. There were also six 5-s blank periods throughout a 5-minute block, the only time during a run that the participants did not press any button. These blank periods were pseudorandomly placed such that they did not appear in the first and the last 30 s of the block and there were at least 25 s of visual stimuli in between two consecutive blank periods.

A 5-minute block could be one of the three conditions: conventional rivalry, replay, or IOS rivalry (see Figure 3.2). The order of these three conditions in a session was fit to a Latin-Square design and the starting condition was counterbalanced between subjects. At the beginning of the first binocular rivalry session, while the T1-weighted image of their brain was obtained, participants completed a practice

47

conventional rivalry block. Across all the binocular rivalry sessions, I aimed at collecting 10 blocks of scans for each of the three conditions. However, some blocks could not be used due to screen flip errors, resulting in glitches in the dichoptic presentation, and were mostly replaced at the end of the session, or at the beginning of the subject's next session. In the analysis, there were nine rivalry and nine replay blocks for S2 and eight IOS rivalry blocks for S3, otherwise there were 10 blocks for each condition for each subject.
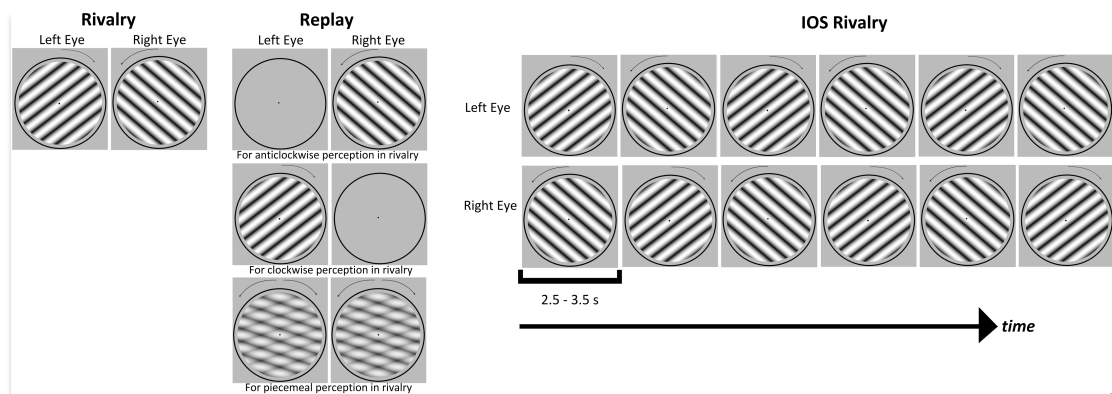
Figure 3.2: The Stimulus Presentation for the Binocular Rivalry Conditions. Rivalry was the conventional binocular rivalry paradigm in which each eye is presented with a different stimulus, rotations counterbalanced across eyes in the actual experiment. Replay was the physical alternations of the stimuli matching with the perceptual reports of the observer during a previous rivalry condition. IOS Rivalry was the interocular switch paradigm in which the rivalry stimuli swap between the eyes in every few seconds, randomly chosen between 2.5-3.5 s.

3.2.2.1.1 Rivalry

The conventional rivalry condition, which will be referred as rivalry from now on, is illustrated in Figure 3.2. Each eye was presented with a grating, rotating as

opposed to each other. Each sinusoidal grating, rotating at $\omega = 1$ cycles/second, was 12° of visual angle in diameter, had spatial frequency of 4 cycles/degree, and shown at full contrast. Each was framed by a black circle, measuring 12.5° in diameter, and presented on a neutral gray background. The clockwise and counterclockwise gratings were counterbalanced between the eyes across rivalry blocks, the initial order also counterbalanced across subjects.

3.2.2.1.2 Replay

Replay was a control condition for the conventional rivalry. The participant's reports from a previous rivalry block were used to mimic their perception. If it was the first block for replay, then the reports from the practice rivalry run were used. This was because of the Latin-square design for the order of the conditions where the first replay block was not always preceded by a conventional rivalry run. As illustrated in Figure 3.2, to mimic the subject's clockwise perception in rivalry, the clockwise rotating grating was presented to the corresponding eye while the other eye was presented with the blank screen in replay. Similarly, if the participant reported counterclockwise rotation in rivalry, then the counterclockwise rotating grating was shown to the matching eye while the other eye was presented with the blank in replay. For the reports of mixture perception in rivalry, the two rotations, superimposed on each other at half transparency, were shown to both eyes in replay. The blank periods in replay were also kept the same as in the matching rivalry block.

3.2.2.1.3 Interocular Switch Rivalry

IOS rivalry was the same as rivalry except there was an interocular switch of the stimuli (see Figure 3.2). In the literature, IOS rivalry paradigms used stable

orthogonal gratings that were flickering at a high frequency (e.g., 18 Hz) and swapping across the eyes every three times in a second (e.g., Denison & Silver, 2012; Logothetis et al., 1996). For the current study, flickering the rotating stimuli hindered the perception of rotation drastically and thus giving rotation responses were confusing. In addition, rotation already adds a temporal property to the stimulus; therefore, the stimuli in IOS rivalry were not flickering. For the eye swap interval of the stimulus, there were a couple restrictions in the decision process. First, the swap interval had to be more than 1 s, the time for a 360° rotation, to perceive a stable rotation long enough to be able to respond. Second, the swap intervals had to be irregular because a fixed interval resulted in a dull plaid perception of rotations, always touching each other at the same point and rotating backwards at regular intervals. Therefore, the opposing gratings in IOS rivalry blocks swapped between the two eyes in every few seconds which was randomly chosen between 2.5 and 3.5 seconds for each swap.

3.2.2.2   Data Processing

To pre-process the functional data from the binocular rivalry sessions, motion correction using MCFLIRT, intensity normalization, high-pass temporal filtering, and no spatial smoothing was applied. The motion outlier volumes were identified with the fsl_motion_outliers command, thresholded at the 75th percentile + 1.5 times the interquartile range.

First, the fMRI data for each rivalry and replay block were analyzed with a GLM. Two EVs, LE perception and RE perception, were defined based on the participant's perceptual reports. Mixture perceptions were included in both EVs. Also, the motion outlier volumes were added to the model as a confound variable. All the

possible contrasts were computed between the two main EVs. Finally, a fixed-effects analysis was conducted for each participant to combine all the rivalry and replay blocks, with all the possible contrasts between the rivalry and replay conditions.

Second, for region-of-interest (ROI) analysis, the GLM results for rivalry–replay contrast were inspected in the M and P sections of each LGN, identified by the qT1 analysis (see Section 1.3.2). The significance threshold was uncorrected for multiple comparisons of voxels as they were analyzed only in the LGN. In addition, using the B weights, a suppression index for each voxel was calculated. Collapsed across LE and RE, the difference in a voxel's response to rivalry and to replay (rivalry–replay) was divided by the sum of its responses to both (rivalry+replay). An index around 0 indicates a successful suppression during perceptual alternations induced by rivalry, similar to those induced by physical alternations in replay.

Finally, to inspect whether the perceptual alternations between the eyes were reflected in the eye-specific regions of LGN, a time series analysis was conducted for the rivalry and the replay conditions. The contralateral (CL) and the ipsilateral (IL) voxels were selected based on the GLM analysis of the eye localizer tasks (described in Section 1.2.2.3). I chose the voxels that responded to one eye significantly more than the other eye in the GLM analysis of both eye localizer tasks (see Figure 1.5b). This decision was due to the match between these voxels and the voxels that were identified based on the unsupervised analysis (see Section 2.3). Then, for each of the CL and IL eye voxels in each LGN, the preprocessed fMRI activity during rivalry and replay was converted to percent change from its average baseline activity. The baseline corresponded to the blank screens, but it was delayed by 6 s (i.e., 4 volumes with the 1.5 s TR) to account for the hemodynamic delay. The data was then

upsampled on the time dimension so that each time point represented 100 ms instead of 1.5 s. The difference in the percent fMRI signal for exclusive CL vs IL eye perceptions were analyzed for the time between 5 seconds before and 15 s after when the participant reported perceiving a single rotation. This analysis could not be carried separately for the contralateral M and the contralateral P layers because these layers could not be identified by the eye localizer tasks (see Chapter 1 and 2).

There was no fMRI data processing for the IOS rivalry condition as it did not yield stimulus and eye rivalry (see Section 3.3.1 below).

3.3 Results

3.3.1 Perceptual Findings

Perceptual reports from participants were analyzed for the distribution of perceptual resolution during rivalry, replay, and IOS. Based on the participants' key press responses, the durations of exclusive perception on a single rotation, or on a single eye, were calculated and concatenated across all the blocks for each condition. Histograms of those perceptual durations can be found in Figure 3.3. As expected, and evident in the figure, rivalry and replay conditions resulted in similar perceptual reports; thus, only rivalry condition is reported in this section. The average exclusive perception was around 7 s across subjects, means ranging from 4.45 s to 8.81 s. The durations for the perceived clockwise vs counterclockwise rotations did not differ. However, the RE perceptions were longer than the LE perceptions for two out of three participants, $t(257) = 4.12$, $p_{Bonf} < .001$, $d = .52$ for S2 and $t(292) = 4.23$, $p_{Bonf} < .001$, $d = .49$ for S3. During the IOS rivalry condition, on the other hand, one of these subjects (S2) experienced longer LE perceptions instead, $t(551) = 3.46$, $p_{Bonf} = .002$, d

= .31, and the other subject (S3) experienced longer clockwise perceptions compared to the counterclockwise perceptions, $t(272) = 2.43$, $p_{Bonf} = .047$, $d = .29$ for S3.
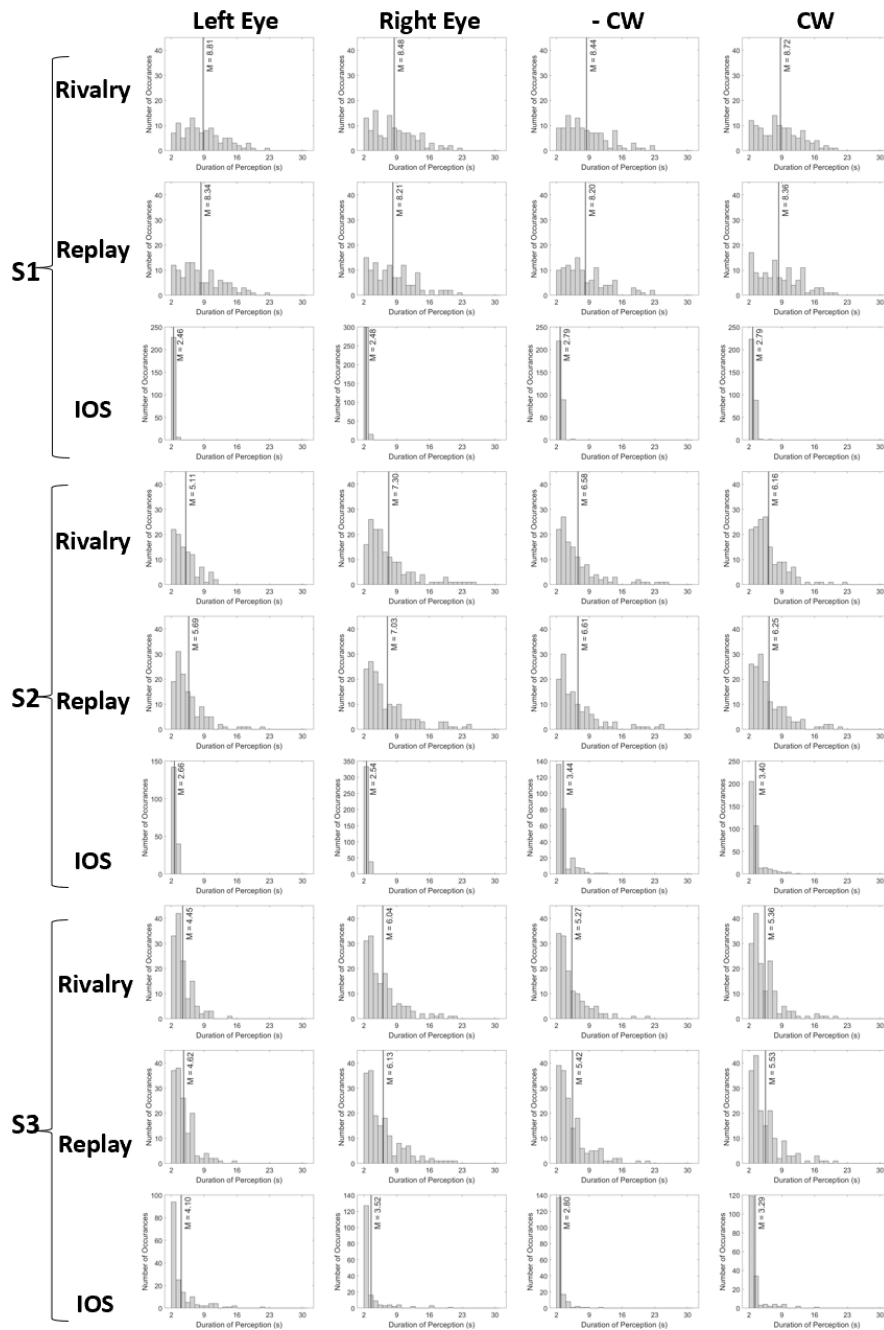
Figure 3.3: Histograms for Perceptual Durations during Binocular Rivalry Experiments. CW: Clockwise rotation, -CW: Counterclockwise rotation, IOS: Interocular switch rivalry. Black lines reflect the mean duration. Bin interval is 1 s.

As can be seen in the distributions in Figure 3.3, the perceptual reports demonstrated no stimulus rivalry in the IOS condition. Neither the number of occurrences (y-axis) nor the perceptual durations (the distribution and the black lines) were similar to the rivalry condition. In fact, the perception was failed to be resolved on a single rotation, or on a single eye, most of the time during IOS rivalry. This is illustrated in the pie charts for the number of eye swaps in Figure 3.4. Stimulus rivalry was calculated as the eye swaps that went unnoticed, indicated by the exclusive perception of a rotation by the time the swap had happened. Eye rivalry, on the other hand, was the eye swaps that were noticed, indicated by the initiation of an exclusive perception following the eye swap within 500 ms. As evident in Figure 3.4, there was neither eye rivalry nor stimulus rivalry, instead, the reported perception was mostly the mixture of the two rotations. Therefore, further analysis for IOS rivalry could not be carried for eye vs stimulus rivalry comparisons.
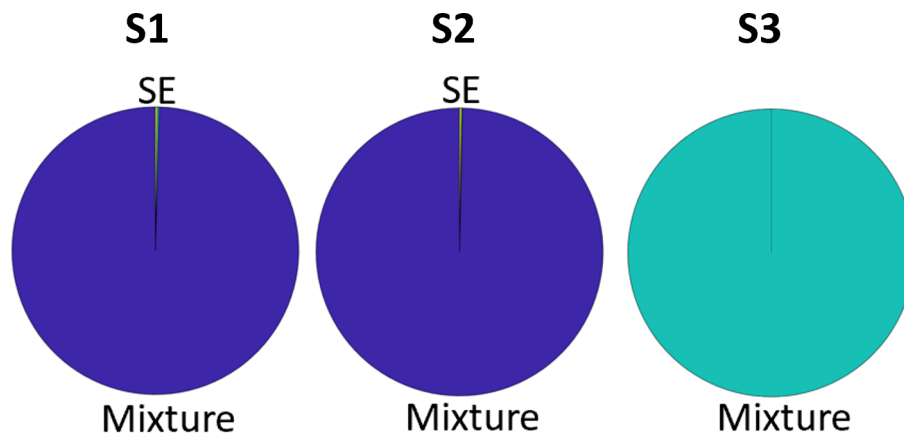

Figure 3.4: Pie Charts for Eye Swaps During Interocular Switch Rivalry. S refers to stimulus rivalry and reflects the number of non-perceived eye swaps. E refers to eye rivalry and reflects the number of perceived eye swaps. Mixture is the number of eye swaps that happened while the participant reported mixture perception.

3.3.2 Rivalry in the M and P Regions of LGN

The GLM results were examined within each LGN to see if there were differences in the overall activity during rivalry and replay blocks. First, rivalry and replay activated similar number of voxels within each LGN and their M and P regions, as indicated by the z-scores (see Figure 3.5a). There were small number of voxels that were significantly more active during rivalry (white voxels) or during replay (black voxels). As can be seen in Figure 3.5a, these significant voxels were spread evenly across the M (area below the red line) and P regions (area above the red line).

Second, there was similar levels of overall suppression in each LGN, demonstrated by the suppression indices around 0 (see Figure 3.5b). I conducted a Bayesian one sample t-test for each LGN and for their M and P parts to see the likelihood of data favoring the null hypothesis (i.e., index not different than 0) over the alternative hypothesis (i.e., index different than 0). Bayesian factors favored the null hypothesis at least moderately across all LGN, *BF01*'s > 8 for LGN, *BF01*'s > 5.5 for P regions, and *BF01*'s > 5 for five out of six M regions. The only ROI that the Bayesian factor favored the alternative hypothesis was S2 right LGN's M section, *BF10* = 11.8. The suppression index was positive in this M section, indicating higher relative activation during rivalry and thus incomplete suppression (see Figure 3.5b). Last, a Bayesian independent samples t-test was employed on the indices to find how likely the data supports the alternative hypothesis that the suppression index is different in the M and P sections of the LGN over the null hypothesis. Bayesian factors revealed that the odds were moderately in favor of the null hypothesis, *BF01*'s > 3.5 for all LGN, indicating similar levels of suppression in the M and P sections.
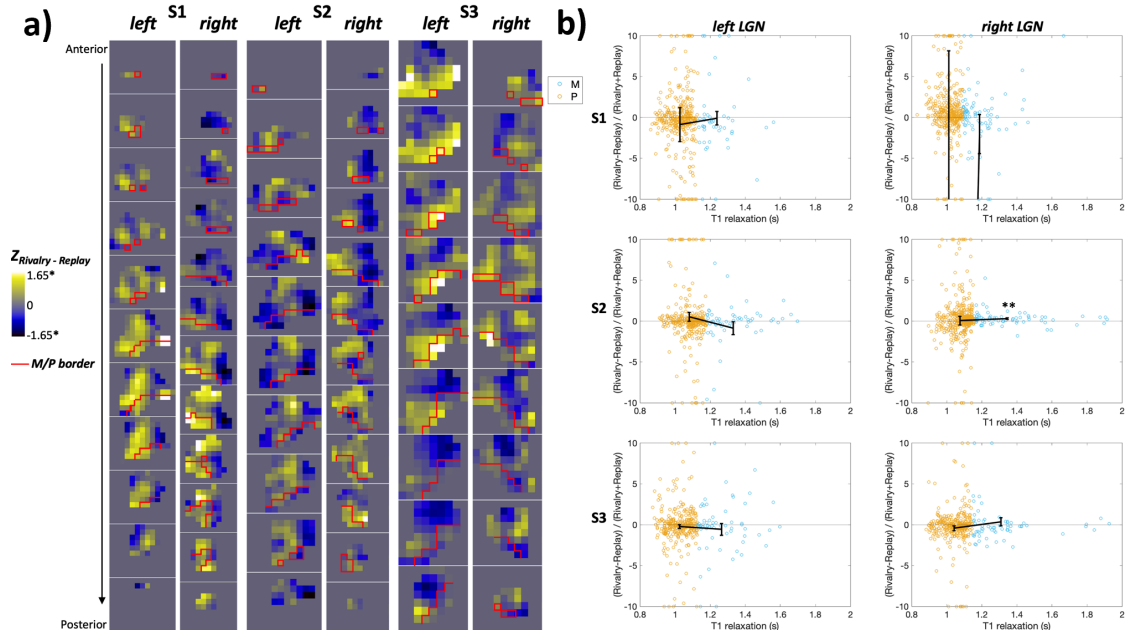
Figure 3.5: GLM Results for Rivalry in the M and P Regions of LGN. a) Coronal slices of each LGN showing the z scores for rivalry vs replay contrast. Red line is where the M and P regions were separated at according to their qT1 values. *$p < .05$, uncorrected for multiple comparisons for voxels. b) Scatterplots of the M and P voxels, indicated by their qT1 values on the x-axis, showing similar suppression for rivalry and replay. The suppression index on the y-axis was calculated by the B weights. For illustration purposes, the voxels with indices beyond 10 and -10 were fixed at 10 and -10 respectively. Black lines indicate the mean index values for M and P voxels, calculated without the range constraint on the suppression index. Error bars are the SEM. **$p = .02$, Bonferroni corrected for six LGN.

3.3.3   Rivalry in the Eye-specific Regions of LGN

The time series analysis of CL and IL voxels in each LGN are visualized in Figure 3.6 for exclusive CL and IL perceptions that lasted more than 6 s. This minimum limit on the perceptual duration was determined to make sure that the fMRI responses were stable enough. This value was around the average exclusive duration across subjects during rivalry (see Section 3.3.1 and Figure 3.3) and corresponded to 4

time points in our original data (with TR being 1.5 s). To compare the responses of CL and IL regions of LGN to perceptual resolution during rivalry and replay, the oscillations after time 0 were inspected to find when the CL eye voxels (blue line) and the IL eye voxels (red line) separated from each other, such that the former is positive on the y-axis while the latter is negative. This would indicate that the CL (IL, respectively) voxels showed increased activity following the perceptual resolution on the CL (IL) eye while showing suppressed activity following the perceptual resolution on the IL (CL) eye.

As can be seen in Figure 3.6, rivalry and replay conditions did not yield similar results. The rivalry condition resulted in more separable oscillations of eye-specific voxels for three LGN, all of which were consistent in their eye-specific region analysis in the previous chapters (S1 right LGN, S3 left and right LGN). Focusing only on these LGN and only for the tendencies of the signals, the oscillations demonstrated signs of the exclusive perception a bit earlier and longer for the rivalry than the replay condition. The LGN that had few numbers of significant eye-specific voxels (S1 left LGN and S2 right LGN, see Figure 1.5b) showed more variance, as evident by the larger 95% confidence intervals (CIs) in Figure 3.6.

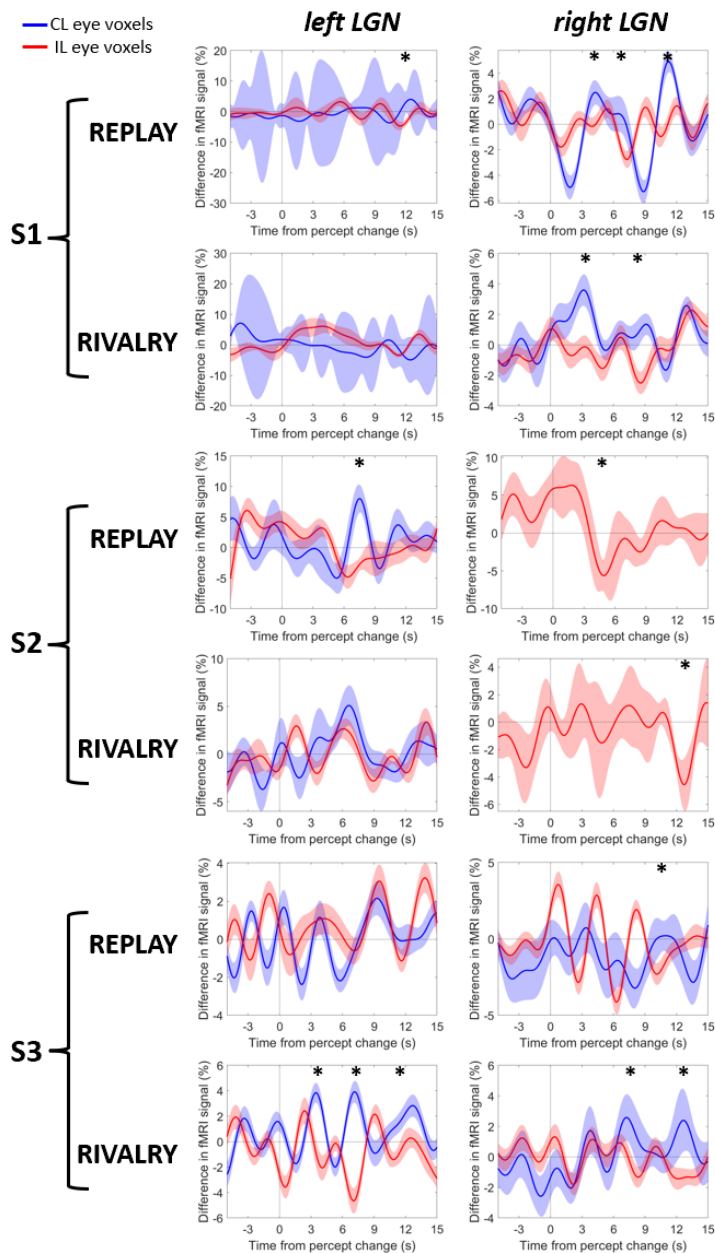Figure 3.6: fMRI Activity around the Exclusive Eye Perceptions during Rivalry and Replay. The x-axis shows the time around when the exclusive perception started (time 0), indicated by the subject's perceptual reports. The y-axis shows the difference in the percent fMRI signal for the contralateral eye perceptions vs ipsilateral eye perceptions. Error shades are 95% confidence intervals. *$p < .05$

3.4   Discussion

I conducted the first neuroimaging study to directly test whether BR is associated with the P pathway more than the M pathway in the brain (Denison & Silver, 2012; He et al., 2005). By analyzing the overall fMRI activity of each participant's LGN, I found similar responses in the disjoint M and P layers to perceptual alternations induced by rivalry vs replay, failing to support the hypothesis. To see whether perception during rivalry was reflected in the LGN, I examined the time series responses and found that the activity in the eye-specific regions represented the perceived eye during rivalry. As discussed in Chapters 1 and 2, the identification of the eye-specific structure in the LGN was found in clusters, not in layers so to separate into M and P; therefore, I could not compare the eye-specific rivalry responses in the M and P sections. Also, the IOS paradigm did not elicit enough perceptual resolution to be examined to test whether the stimulus rivalry is associated with the P and the eye rivalry is associated with the M pathway (Denison & Silver, 2012).

The similar suppression during rivalry and replay for the M and P layers of LGN indicated no bias of the two visual pathways for perceptual alternations induced by rivalry. Instead, the distribution of rivalry and replay related activity in the LGN seems to show a structure that resembles to the retinotopic map in LGN representing the visual eccentricity (DeSimone et al., 2015; Schneider et al., 2004), such that the replay activated areas that corresponded to central field and the rivalry activated areas that corresponded to the surround field of the stimulus. One possible explanation could be the difference in the mixture perception induced by rivalry and replay. The large rivalry stimuli might have resulted in different center-surround rotations which were indicated as the mixture perception by the participants whereas the mixture of

rotations was homogeneous in the replay stimuli. However, I did not localize the retinotopic maps with an eccentricity manipulation in the visual stimulus; thus, this conclusion cannot be drawn with the current data.

Consistent with the previous investigations of rivalry in the LGN (Haynes et al., 2005; Wunderlich et al., 2005), the perception was reflected in the LGN even though the color confound in the stimulus was eliminated in the present research. However, the eye-specific responses to the exclusive eye perceptions were not as pronounced or prolonged in my study compared to Haynes et al's (2005). The stimuli in Haynes et al. (2005) were blue/red gratings that started rotating in the same direction orthogonally. It is possible that rivalry resolved better on one of the colors as the rotation in their study supported coherent and long perceptions (Blake et al., 2003) while motion opponency in our study prevented building coherent perceptions. Consistent with this, the average exclusive perception in this research was 3 s shorter than what they reported. However, it should be noted that Haynes et al. (2005) did not give an option to report mixture perception. Also, there was no control condition in Haynes et al.'s (2005) study to compare the eye-specific responses for perceptual and physical alternations. In this study, the control replay condition, nevertheless, was not a valid control for the time series activity. The eye-specific activity with the replay stimulus was not as clear as with the rivalry stimulus which could be driven by the motion adaptation and the resulting motion after-effects during replay.

This study showed that, with the rotation-opponent achromatic gratings, the perception can be resolved on one rotation long enough to be analyzed for fMRI responses. There has been reports of longer perceptions of rotating rivalry stimuli, but these studies had more global rotations such as spirals or radial gratings (Carlson &

He, 2000; Malek et al., 2012; Nguyen et al., 2003). Also, I found a RE dominance during rivalry for two out of three participants, as indicated by the longer exclusive perceptions for the RE than the LE. These participants reported having different dominant eyes in the simple sighting tests. Correlations between the dominant eye in sighting and the dominant eye in perception during rivalry were reported before (Handa et al., 2004; Porac & Coren, 1978); yet, it has been also suggested that it is the sensory eye dominance that the binocular rivalry measures, which is not related to the sighting eye dominance (Dieter et al., 2017). The present study, with its small sample, supported the latter conclusion.

When the rotating gratings swapped between the eyes in the IOS paradigm, there was no perceptual resolution on a grating, or on an eye. The previous research with IOS paradigm used orthogonal gratings that swapped between the eyes in a fast fashion while flickering rapidly to cover this eye swap and to result in more stimulus rivalry (e.g., Bhardwaj & O'Shea, 2012; Denison & Silver, 2012; S. H. Lee & Blake, 1999; Logothetis et al., 1996; V. Patel et al., 2015; Silver & Logothetis, 2007). With a similar procedure and simple stimuli, Christiansen et al. (2017) found that the stimuli that differed only in color result in more stimulus rivalry than the stimuli that differed in luminance which did not produce perceptual alternations at all. Luminance is processed by the M neurons as is motion in the current study. This suggests that the M-stimuli might not be optimal for generating slow stimulus alternations (Denison & Silver, 2012; He et al., 2005). Nevertheless, the motion stimuli I used were more complex than their luminance stimuli and required more global processing, engaging both M and P neurons. There was the direction of rotation as well as the regular changes in the orientation of the sinusoidal gratings across the retinal images. Perhaps,

the rotations were interrupted by the eye swap too visibly for either eye, leading to the mixture of rotations dominating the perception instead of perceptual resolution. Previously, in their investigation of the complexity of the stimuli on perceptual resolution, Sandberg et al. (2011) used an eye-swapping procedure with the flickering stimuli as well as with a blank screen before each eye swap. They found perceptual resolutions on the eye which was not disrupted by the eye swaps between the complex stimuli (i.e., faces/houses) while the eye-swaps between simple stimuli (i.e., orthogonal gratings, not rotating) disrupted the perceptual alternations. However, this was the case even when they scrambled their complex stimuli, suggesting an importance for the overlaps at lower-level features. Thus, the rotating stimuli in the current study, changing the overlap in the retinal position more frequently, may not be optimal to resolve the binocular competition with the eye-swapping procedure.

3.4.1 Conclusion

Overall, this study demonstrated that the rotation-opponent rivalry stimuli could be used to inspect the LGN responses that were not dependent on color-opponency. Even though the rivalry results for LGN were interpretable to conclude that the M and P activity were similarly suppressed and the activity changes in the eye-specific regions reflected the perceived changes during rivalry, caveats are suggested as the control replay condition could yield different perceptual experiences with large motion stimuli.

REFERENCES

Abbie, A. A. (1933). The blood supply of the lateral geniculate body, with a note on the morphology of the choroidal arteries. *Journal of Anatomy*, *67*(Pt 4), 521. https://www.ncbi.nlm.nih.gov/pmc/articles/PMC1249321/

Aggarwal, P., & Gupta, A. (2018). Low rank and sparsity constrained method for identifying overlapping functional brain networks. *PLOS ONE*, *13*(11), e0208068. https://doi.org/10.1371/JOURNAL.PONE.0208068

Alais, D., & Blake, R. (2015). Binocular rivalry and perceptual ambiguity. In J. Wagemans (Ed.), *Oxford handbook of perceptual organization* (pp. 775–798). Oxford University Press. https://doi.org/10.3758/BF03198843

Alais, D., O'Shea, R. P., Mesana-Alais, C., & Wilson, I. G. (2000). On binocular alternation. *Perception*, *29*(12), 1437–1445. https://doi.org/10.1068/p3017

Aldusary, N., Michels, L., Traber, G. L., Hartog-Keisker, B., Wyss, M., Baeshen, A., Huebel, K., Almalki, Y. E., Brunner, D. O., Pruessmann, K. P., Landau, K., Kollias, S., & Piccirelli, M. (2019). Lateral geniculate nucleus volumetry at 3T and 7T: Four different optimized magnetic-resonance-imaging sequences evaluated against a 7T reference acquisition. *NeuroImage*, *186*, 399–409. https://doi.org/10.1016/J.NEUROIMAGE.2018.09.046

Aleci, C., & Belcastro, E. (2016). Parallel convergences: A glimpse to the magno-And parvocellular pathways in visual perception. *World Journal of Research and Review*, *3*(3), 34–42.

Andrews, T. J., Halpern, S. D., & Purves, D. (1997). Correlated Size Variations in Human Visual Cortex, Lateral Geniculate Nucleus, and Optic Tract. *Journal of Neuroscience*, *17*(8), 2859–2868. https://doi.org/10.1523/JNEUROSCI.17-08-02859.1997

Andrews, T. J., & Purves, D. (1997). Similarities in normal and binocularly rivalrous viewing. *Proceedings of the National Academy of Sciences of the United States of America*, *94*(18), 9905–9908. https://doi.org/10.1073/PNAS.94.18.9905

Bhardwaj, R., & O'Shea, R. P. (2012). Temporal analysis of image-rivalry suppression. *PLOS ONE*, *7*(9), e45407. https://doi.org/10.1371/JOURNAL.PONE.0045407

Bhardwaj, R., O'Shea, R. P., Alais, D., & Parker, A. (2008). Probing visual consciousness: rivalry between eyes and images. *Journal of Vision*, *8*(11), 2.1-13. https://doi.org/10.1167/8.11.2

Blake, R. (1989). A neural theory of binocular rivalry. *Psychological Review*, *96*(1), 145–167. https://doi.org/10.1037/0033-295X.96.1.145

Blake, R., Brascamp, J., & Heeger, D. J. (2014). Can binocular rivalry reveal neural correlates of consciousness? *Philosophical Transactions of the Royal Society B: Biological Sciences*, *369*(1641). https://doi.org/10.1098/rstb.2013.0211

Blake, R., & Fox, R. (1974). Binocular rivalry suppression: Insensitive to spatial frequency and orientation change. *Vision Research*, *14*(8), 687–692. https://doi.org/10.1016/0042-6989(74)90065-0

Blake, R., & Logothetis, N. K. (2002). Visual competition. *Nature Reviews Neuroscience*, *3*, 13–21. https://doi.org/10.1038/nrn701

Blake, R., Sobel, K. v., & Gilroy, L. A. (2003). Visual motion retards alternations between conflicting perceptual interpretations. *Neuron*, *39*(5), 869–878. https://doi.org/10.1016/S0896-6273(03)00495-1

Blake, R., Westendorf, D. H., & Overton, R. (1980). What is suppressed during binocular rivalry? *Perception*, *9*(2), 223–231. https://doi.org/10.1068/P090223

Boutsidis, C., & Gallopoulos, E. (2008). SVD based initialization: A head start for nonnegative matrix factorization. *Pattern Recognition*, *41*(4), 1350–1362. https://doi.org/10.1016/J.PATCOG.2007.09.010

Brainard, D. H. (1997). The psychophysics toolbox. *Spatial Vision*, *10*(4), 433–436. https://doi.org/10.1163/156856897X00357

Brascamp, J. W., & Blake, R. (2012). Inattention abolishes binocular rivalry: Perceptual evidence. *Psychological Science*, *23*(10), 1159–1167. https://doi.org/10.1177/0956797612440100

Breitmeyer, B. G. (2014). Contributions of magno- and parvocellular channels to conscious and non-conscious vision. *Philosophical Transactions of the Royal Society B: Biological Sciences*, *369*(1641), 20130213–20130213. https://doi.org/10.1098/rstb.2013.0213

Burke, D., Alais, D., & Wenderoth, P. (1999). Determinants of fusion of dichoptically presented orthogonal gratings. *Perception*, *28*(1), 73–88. https://doi.org/10.1068/P2694

Butler, P. D., & Javitt, D. C. (2005). Early-stage visual processing deficits in schizophrenia. *Current Opinion in Psychiatry*, *18*(2), 151–157. https://doi.org/10.1097/00001504-200503000-00008

Carlson, T. A., & He, S. (2000). Visible binocular beats from invisible monocular stimuli during binocular rivalry. *Current Biology*, *10*(17), 1055–1058. https://doi.org/10.1016/s0960-9822(00)00672-2

Christiansen, J. H., D'Antona, A. D., & Shevell, S. K. (2017). Chromatic interocular-switch rivalry. *Journal of Vision*, *17*(5), 9. https://doi.org/10.1167/17.5.9

Denison, R. N., & Silver, M. A. (2012). Distinct contributions of the magnocellular and parvocellular visual streams to perceptual selection. *Journal of Cognitive Neuroscience*, *24*(1), 246–259. https://doi.org/10.1162/jocn_a_00121

Denison, R. N., Vu, A. T., Yacoub, E., Feinberg, D. A., & Silver, M. A. (2014). Functional mapping of the magnocellular and parvocellular subdivisions of human LGN. *NeuroImage*, *102*(P2), 358–369. https://doi.org/10.1016/j.neuroimage.2014.07.019

Derrington, A. M., & Lennie, P. (1984). Spatial and temporal contrast sensitivities of neurones in lateral geniculate nucleus of macaque. *The Journal of Physiology*, *357*(1), 219–240. https://doi.org/10.1113/JPHYSIOL.1984.SP015498

DeSimone, K., & Schneider, K. A. (2019). Distinguishing hemodynamics from function in the human LGN using a temporal response model. *Vision*, *3*(2), 27. https://doi.org/10.3390/VISION3020027

DeSimone, K., Viviano, J. D., & Schneider, K. A. (2015). Population receptive field estimation reveals new retinotopic maps in human subcortex. *Journal of Neuroscience*, *35*(27), 9836–9847. https://doi.org/10.1523/JNEUROSCI.3840-14.2015

Diaz-Caneja, E. (1928). Sur l'alternance binoculaire [On binocular alternation]. *Annales d'Oculistique*, *165*, 721–731.

Dieter, K. C., Brascamp, J., Tadin, D., & Blake, R. (2016). Does visual attention drive the dynamics of bistable perception? *Attention, Perception, and Psychophysics*, *78*(7), 1861–1873. https://doi.org/10.3758/s13414-016-1143-2

Dieter, K. C., Sy, J. L., & Blake, R. (2017). Individual differences in sensory eye dominance reflected in the dynamics of binocular rivalry. *Vision Research*, *141*, 40–50. https://doi.org/10.1016/J.VISRES.2016.09.014

Fox, R., & Check, R. (1966). Forced-choice form recognition during binocular rivalry. *Psychonomic Science*, *6*(10), 471–472. https://doi.org/10.3758/BF03328096

Freeman, A. W. (2005). Multistage model for binocular rivalry. *Journal of Neurophysiology*, *94*, 4412–4420. https://doi.org/10.1152/jn.00557.2005.

Giraldo-Chica, M., Hegarty, J. P., & Schneider, K. A. (2015). Morphological differences in the lateral geniculate nucleus associated with dyslexia. *NeuroImage: Clinical*, *7*, 830–836. https://doi.org/10.1016/J.NICL.2015.03.011

Handa, T., Mukuno, K., Uozato, H., Niida, T., Shoji, N., & Shimizu, K. (2004). Effects of dominant and nondominant eyes in binocular rivalry. *Optometry and Vision Science*, *81*(5), 377–383. https://doi.org/10.1097/01.opx.0000135085.54136.65

Hassler, R. (1966). Comparative anatomy of the central visual systems in day-and night-active primates. In *Evolution of the Forebrain* (pp. 419–434). Springer, Boston, MA. https://doi.org/10.1007/978-1-4899-6527-1_40

Haynes, J. D., Deichmann, R., & Rees, G. (2005). Eye-specific effects of binocular rivalry in the human lateral geniculate nucleus. *Nature*, *438*(7067), 496–499. https://doi.org/10.1038/nature04169

Haynes, J. D., & Rees, G. (2005). Predicting the stream of consciousness from activity in human visual cortex. *Current Biology*, *15*(14), 1301–1307. https://doi.org/10.1016/j.cub.2005.06.026

He, S., Carlson, T., & Chen, X. (2005). Parallel pathways and temporal dynamics in binocular rivalry. In D. Alais & R. Blake (Eds.), *Binocular rivalry* (pp. 81–100). MIT Press. https://psycnet.apa.org/record/2005-03072-005

Hess, R. F., Thompson, B., Gole, G., & Mullen, K. T. (2009). Deficient responses from the lateral geniculate nucleus in humans with amblyopia. *European Journal*

of *Neuroscience*, *29*(5), 1064–1070. https://doi.org/10.1111/J.1460-9568.2009.06650.X

Jiang, Y., Costello, P., Fang, F., Huang, M., & He, S. (2006). A gender- and sexual orientation-dependent spatial attentional effect of invisible images. *Proceedings of the National Academy of Sciences*, *103*(45), 17048–17052. https://doi.org/10.1073/PNAS.0605678103

Jiang, Y., Costello, P., & He, S. (2007). Processing of invisible stimuli: advantage of upright faces and recognizable words in overcoming interocular suppression. *Psychological Science*, *18*(4), 349–355. https://doi.org/10.1111/J.1467-9280.2007.01902.X

Kastner, S., O'Connor, D. H., Fukui, M. M., Fehd, H. M., Herwig, U., & Pinsk, M. A. (2004). Functional imaging of the human lateral geniculate nucleus and pulvinar. *Journal of Neurophysiology*, *91*(1), 438–448. https://doi.org/10.1152/JN.00553.2003/ASSET/IMAGES/LARGE/9K0143604108.JPEG

Kitajima, M., Hirai, T., Yoneda, T., Iryo, Y., Azuma, M., Tateishi, M., Morita, K., Komi, M., & Yamashita, Y. (2015). Visualization of the medial and lateral geniculate nucleus on phase difference enhanced imaging. *American Journal of Neuroradiology*, *36*(9), 1669–1674. https://doi.org/10.3174/AJNR.A4356

Kovács, I., Papathomas, T. v., Yang, M., & Fehér, Á. (1996). When the brain changes its mind: Interocular grouping during binocular rivalry. *Proceedings of the National Academy of Sciences*, *93*(26), 15508–15511. https://doi.org/10.1073/PNAS.93.26.15508

Lee, D., & Seung, H. S. (2000). Algorithms for non-negative matrix factorization. *Advances in Neural Information Processing Systems*, *13*, 556–562. https://papers.nips.cc/paper/2000/hash/f9d1152547c0bde01830b7e8bd60024c-Abstract.html

Lee, S. H., & Blake, R. (1999). Rival ideas about binocular rivalry. *Vision Research*, *39*(8), 1447–1454. https://doi.org/10.1016/S0042-6989(98)00269-7

Lee, S. H., Blake, R., & Heeger, D. J. (2005). Traveling waves of activity in primary visual cortex during binocular rivalry. *Nature Neuroscience 2004 8:1*, *8*, 22–23. https://doi.org/10.1038/nn1365

Lehky, S. R. (1988). An astable multivibrator model of binocular rivalry. *Perception*, *17*(2), 215–228. https://doi.org/10.1068/P170215

Leopold, D. A., & Logothetis, N. K. (1999). Multistable phenomena: Changing views in perception. *Trends in Cognitive Sciences*, *3*(7), 254–264. https://doi.org/10.1016/S1364-6613(99)01332-7

Levelt, W. J. M. (1965). *On binocular rivalry*. http://pubman.mpdl.mpg.de/pubman/item/escidoc:77195/component/escidoc:2424565/Levelt_Binocular_Rivalry_1965.pdf

Levelt, W. J. M. (1967). Note on the distribution of dominance times in binocular rivalry. *British Journal of Psychology*, *58*(1), 143–145. https://doi.org/10.1111/J.2044-8295.1967.TB01068.X

Li, X., Gan, J. Q., & Wang, H. (2018). Collective sparse symmetric non-negative matrix factorization for identifying overlapping communities in resting-state brain functional networks. *NeuroImage*, *166*, 259–275. https://doi.org/10.1016/J.NEUROIMAGE.2017.11.003

Livingstone, M., & Hubel, D. (1988). Segregation of Form, Color, Movement, and Depth: Anatomy, Physiology, and Perception. *Science*, *240*(4853), 740–749. https://doi.org/10.1126/SCIENCE.3283936

Logothetis, N. K., Leopold, D. A., & Sheinberg, D. L. (1996). What is rivalling during binocular rivalry? [see comments]. *Nature*, *380*(6575), 621–624.

Lutti, A., Dick, F., Sereno, M. I., & Weiskopf, N. (2014). Using high-resolution quantitative mapping of R1 as an index of cortical myelination. *NeuroImage*, *93 Pt 2*, 176–188. https://doi.org/10.1016/J.NEUROIMAGE.2013.06.005

Malek, N., Mendoza-Halliday, D., & Martinez-Trujillo, J. (2012). Binocular rivalry of spiral and linear moving random dot patterns in human observers. *Journal of Vision*, *12*(10), 16–16. https://doi.org/10.1167/12.10.16

Maunsell, J. H. R. (1992). Functional visual streams. *Current Opinion in Neurobiology*, *2*(4), 506–510. https://doi.org/10.1016/0959-4388(92)90188-Q

Merigan, W. H., & Maunsell, J. H. R. (1993). How parallel are the primate visual pathways? *Annual Review of Neuroscience*, *16*, 369–402. https://doi.org/10.1146/ANNUREV.NE.16.030193.002101

Mezer, A., Yeatman, J. D., Stikov, N., Kay, K. N., Cho, N. J., Dougherty, R. F., Perry, M. L., Parvizi, J., Hua, L. H., Butts-Pauly, K., & Wandell, B. A. (2013). Quantifying the local tissue volume and composition in individual brains with magnetic resonance imaging. *Nature Medicine*, *19*(12), 1667–1672. https://doi.org/10.1038/NM.3390

Milner, A. D. (2012). Is visual processing in the dorsal stream accessible to consciousness? *Proceedings of the Royal Society B: Biological Sciences*, *279*(1737), 2289–2298. https://doi.org/10.1098/RSPB.2011.2663

Müller-Axt, C., Eichner, C., Rusch, H., Kauffmann, L., Bazin, P. L., Anwander, A., Morawski, M., & von Kriegstein, K. (2021). Mapping the human lateral geniculate nucleus and its cytoarchitectonic subdivisions using quantitative MRI. *NeuroImage*, *244*, 118559. https://doi.org/10.1016/J.NEUROIMAGE.2021.118559

Nassi, J. J., & Callaway, E. M. (2009). Parallel processing strategies of the primate visual system. *Nature Reviews Neuroscience 2009 10:5*, *10*(5), 360–372. https://doi.org/10.1038/nrn2619

Nguyen, V. A., Freeman, A. W., & Alais, D. (2003). Increasing depth of binocular rivalry suppression along two visual pathways. *Vision Research*, *43*(19), 2003–2008. https://doi.org/10.1016/S0042-6989(03)00314-6

O'Brien, K. R., Kober, T., Hagmann, P., Maeder, P., Marques, J., Lazeyras, F., Krueger, G., & Roche, A. (2014). Robust T1-weighted structural brain imaging and morphometry at 7T using MP2RAGE. *PLOS ONE*, *9*(6), e99676. https://doi.org/10.1371/JOURNAL.PONE.0099676

Oishi, H., Takemura, H., & Amano, K. (2020). Macromolecular tissue volume mapping of lateral geniculate nucleus subdivisions in living human brains. *BioRxiv*, 2020.12.26.424373. https://doi.org/10.1101/2020.12.26.424373

Ooi, T. L., & He, Z. J. (1999). Binocular rivalry and visual awareness: the role of attention. *Perception*, *28*(5), 551–574. https://doi.org/10.1068/P2923

O'Shea, R. P., & Blake, R. (1986). Dichoptic temporal frequency differences do not lead to binocular rivalry. *Perception & Psychophysics*, *39*(1), 59–63. https://doi.org/10.3758/BF03207584

Parkkonen, L., Andersson, J., Hämäläinen, M., & Hari, R. (2008). Early visual brain areas reflect the percept of an ambiguous scene. *Proceedings of the National Academy of Sciences*, *105*(51), 20500–20504. https://doi.org/10.1073/PNAS.0810966105

Patel, R., Steele, C. J., Chen, A. G. X., Patel, S., Devenyi, G. A., Germann, J., Tardif, C. L., & Chakravarty, M. M. (2020). Investigating microstructural variation in the human hippocampus using non-negative matrix factorization. *NeuroImage*, *207*, 116348. https://doi.org/10.1016/J.NEUROIMAGE.2019.116348

Patel, V., Stuit, S., & Blake, R. (2015). Individual differences in the temporal dynamics of binocular rivalry and stimulus rivalry. *Psychonomic Bulletin & Review*, *22*(2), 476–482. https://doi.org/10.3758/s13423-014-0695-1

Pistorio, A. L., Hendry, S. H., & Wang, X. (2006). A modified technique for high-resolution staining of myelin. *Journal of Neuroscience Methods*, *153*(1), 135–146. https://doi.org/10.1016/J.JNEUMETH.2005.10.014

Polonsky, A., Blake, R., Braun, J., & Heeger, D. J. (2000). Neuronal activity in human primary visual cortex correlates with perception during binocular rivalry. *Nature Neuroscience*, *3*(11), 1153–1159. https://doi.org/10.1038/80676

Porac, C., & Coren, S. (1978). Sighting Dominance and Binocular Rivalry. *Optometry and Vision Science*, *55*(3), 208–213.

Qian, Y., Zou, J., Zhang, Z., An, J., Zuo, Z., Zhuo, Y., Wang, D. J. J., & Zhang, P. (2020). Robust functional mapping of layer-selective responses in human lateral geniculate nucleus with high-resolution 7T fMRI. *Proceedings of the Royal Society B*, *287*(1925). https://doi.org/10.1098/RSPB.2020.0245

Rees, G. (2009). Neural correlates of visual consciousness. *The Neurology of Consciousness: Cognitive Neuroscience and Neuropathology*, 61–70. https://doi.org/10.1016/B978-0-12-800948-2.00004-2

Robert, C., Patel, R., Blostein, N., Steele, C. C., & Chakravarty, M. M. (2022). Analyses of microstructural variation in the human striatum using non-negative matrix factorization. *NeuroImage*, *246*, 118744. https://doi.org/10.1016/J.NEUROIMAGE.2021.118744

Sandberg, K., Bahrami, B., Lindeløv, J. K., Overgaard, M., & Rees, G. (2011). The impact of stimulus complexity and frequency swapping on stabilization of binocular rivalry. *Journal of Vision*, *11*(2). https://doi.org/10.1167/11.2.6

Schechter, I., Butler, P. D., Silipo, G., Zemon, V., & Javitt, D. C. (2003). Magnocellular and parvocellular contributions to backward masking dysfunction

in schizophrenia. *Schizophrenia Research*, *64*(2–3), 91–101. https://doi.org/10.1016/S0920-9964(03)00008-2

Schneider, K. A., Richter, M. C., & Kastner, S. (2004). Retinotopic organization and functional subdivisions of the human lateral geniculate nucleus: A high-resolution functional magnetic resonance imaging study. *Journal of Neuroscience*, *24*(41), 8975–8985. https://doi.org/10.1523/JNEUROSCI.2413-04.2004

Selemon, L. D., & Begovic′, A. (2007). Stereologic analysis of the lateral geniculate nucleus of the thalamus in normal and schizophrenic subjects. *Psychiatry Research*, *151*(1–2), 1–10. https://doi.org/10.1016/J.PSYCHRES.2006.11.003

Shapley, R., & Perry, V. H. (1986). Cat and monkey retinal ganglion cells and their visual functional roles. *Trends in Neurosciences*, *9*(C), 229–235. https://doi.org/10.1016/0166-2236(86)90064-0

Shlens, J. (2014a). A tutorial on principal component analysis. *ArXiv*. https://doi.org/10.48550/arxiv.1404.1100

Shlens, J. (2014b). A tutorial on independent component analysis. *ArXiv*. https://doi.org/10.48550/arxiv.1404.2986

Silver, M. A., & Logothetis, N. K. (2007). Temporal frequency and contrast tagging bias the type of competition in interocular switch rivalry. *Vision Research*, *47*(4), 532–543. https://doi.org/10.1016/j.visres.2006.10.011

Skalicky, S. E. (2016). The lateral geniculate nucleus. In *Ocular and visual physiology* (pp. 201–206). Springer, Singapore. https://doi.org/10.1007/978-981-287-846-5_13

Sotiras, A., Resnick, S. M., & Davatzikos, C. (2015). Finding imaging patterns of structural covariance via non-negative matrix factorization. *NeuroImage*, *108*, 1–16. https://doi.org/10.1016/J.NEUROIMAGE.2014.11.045

Stein, J. (2001). The magnocellular theory of developmental dyslexia. *Dyslexia*, *7*(1), 12–36. https://doi.org/10.1002/DYS.186

Stein, J., & Walsh, V. (1997). To see but not to read: The magnocellular theory of dyslexia. *Trends in Neurosciences*, *20*(4), 147–152. https://doi.org/10.1016/S0166-2236(96)01005-3

Tong, F. (2001). Competing theories of binocular rivalry: A possible resolution. *Brain and Mind*, *2*(1), 55–83. http://resolver.scholarsportal.info/resolve/13891987/v02i0001/55_ctobrapr.xml

Tong, F. (2003). Primary visual cortex and visual awareness. *Nature Reviews Neuroscience*, *4*(3), 219–229. https://doi.org/10.1038/nrn1055

Tong, F., & Engel, S. A. (2001). Interocular rivalry revealed in the human cortical blind-spot representation. *Nature*, *411*(May), 195–199. https://doi.org/10.1038/35075583

Tong, F., Meng, M., & Blake, R. (2006). Neural bases of binocular rivalry. *Trends in Cognitive Sciences*, *10*(11). https://doi.org/10.1016/j.tics.2006.09.003

Türkmen, A. C. (2015). A review of nonnegative matrix factorization methods for clustering. *ArXiv*. https://doi.org/10.48550/arxiv.1507.03194

Wade, N. J., & Wenderoth, P. (1978). The influence of colour and contour rivalry on the magnitude of the tilt after-effect. *Vision Research*, *18*(7), 827–835. https://doi.org/10.1016/0042-6989(78)90123-2

Wales, R., & Fox, R. (1970). Increment detection thresholds during binocular rivalry suppression. *Perception & Psychophysics*, *8*(2), 90–94.

Wang, J., Miao, W., Li, J., Li, M., Zhen, Z., Sabel, B., Xian, J., & He, H. (2015). Automatic segmentation of the lateral geniculate nucleus: Application to control and glaucoma patients. *Journal of Neuroscience Methods*, *255*, 104–114. https://doi.org/10.1016/J.JNEUMETH.2015.08.006

Wilson, H. R. (2003). Computational evidence for a rivalry hierarchy in vision. *Proceedings of the National Academy of Sciences*, *100*(24), 14499–14503. https://doi.org/10.1073/PNAS.2333622100

Wolfe, J. M. (1986). Stereopsis and binocular rivalry. *Psychological Review*, *93*(3), 269–282. https://doi.org/10.1037/0033-295X.93.3.269

Wunderlich, K., Schneider, K. A., & Kastner, S. (2005). Neural correlates of binocular rivalry in the human lateral geniculate nucleus. *Nature Neuroscience*, *8*(11), 1595–1602. https://doi.org/10.1038/nn1554

Yang, Z., & Oja, E. (2010). Linear and nonlinear projective nonnegative matrix factorization. *IEEE Transactions on Neural Networks*, *21*(5), 734–749. https://doi.org/10.1109/TNN.2010.2041361

Zhang, P., Jamison, K., Engel, S., He, B., & He, S. (2011). Binocular rivalry requires visual attention. *Neuron*, *71*(2), 362–369. https://doi.org/10.1016/J.NEURON.2011.05.035

Zhang, P., Zhou, H., Wen, W., & He, S. (2015). Layer-specific response properties of the human lateral geniculate nucleus and superior colliculus. *NeuroImage*, *111*. https://doi.org/10.1016/j.neuroimage.2015.02.025

Zhou, G., Zhang, L., Liu, J., Yang, J., & Qu, Z. (2010). Specificity of face processing without awareness. *Consciousness and Cognition*, *19*(1), 408–412. https://doi.org/10.1016/J.CONCOG.2009.12.009

Appendix A

INSTITUTIONAL REVIEW BOARD PROJECT APPROVAL

Institutional Review Board
210H Hullihen Hall
Newark, DE 19716
Phone: 302-831-2137
Fax: 302-831-2828

DATE: September 9, 2019

TO: Keith Schneider
FROM: University of Delaware IRB

STUDY TITLE: [1472937-1] Binocular rivalry
SUBMISSION TYPE: New Project

ACTION: APPROVED
EFFECTIVE DATE: September 9, 2019
NEXT REPORT DUE: September 8, 2020

REVIEW TYPE: Expedited Review
REVIEW CATEGORY: Expedited review category # *(4,7)*

Thank you for your New Project submission to the University of Delaware Institutional Review Board (UD IRB). The UD IRB has reviewed and APPROVED the proposed research and submitted documents via Expedited Review in compliance with the pertinent federal regulations.

As the Principal Investigator for this study, you are responsible for, and agree that:

- All research must be conducted in accordance with the protocol and all other study forms as approved in this submission. Any revisions to the approved study procedures or documents must be reviewed and approved by the IRB prior to their implementation. Please use the UD amendment form to request the review of any changes to approved study procedures or documents.
- Informed consent is a process that must allow prospective participants sufficient opportunity to discuss and consider whether to participate. IRB-approved and stamped consent documents must be used when enrolling participants and a written copy shall be given to the person signing the informed consent form.
- Unanticipated problems, serious adverse events involving risk to participants, and all non-compliance issues must be reported to this office in a timely fashion according with the UD requirements for reportable events. All sponsor reporting requirements must also be followed.

The UD IRB REQUIRES the submission of a PROGRESS REPORT DUE ON September 8, 2020. A continuing review/progress report form must be submitted to the UD IRB at least 45 days prior to the due date to allow for the review of that report.

If you have any questions, please contact the UD IRB Office at (302) 831-2137 or via email at hsrb-research@udel.edu. Please include the study title and reference number in all correspondence with this office.

INSTITUTIONAL REVIEW BOARD

- 1 -   Generated on IRBNet

72

Appendix B

INSTITUTIONAL REVIEW BOARD AMENDMENT APPROVAL 1

Institutional Review Board
210H Hullihen Hall
Newark, DE 19716
Phone: 302-831-2137
Fax: 302-831-2828

DATE: November 11, 2020

TO: Keith Schneider
FROM: University of Delaware IRB

STUDY TITLE: [1472937-3] Binocular rivalry
SUBMISSION TYPE: Amendment/Modification

ACTION: APPROVED
EFFECTIVE DATE: November 11, 2020
NEXT REPORT DUE: September 8, 2021

REVIEW TYPE: Expedited Review
REVIEW CATEGORY: Expedited review category # *(4,7)*

Thank you for your Amendment/Modification submission to the University of Delaware Institutional Review Board (UD IRB). The UD IRB has reviewed and APPROVED the proposed research and submitted documents via Expedited Review in compliance with the pertinent federal regulations.

Please continue to reference https://research.udel.edu/coronavirus for the most up-to-date recommendations regarding in-person research interaction with subjects during the COVID-19 national emergency.

As the Principal Investigator for this study, you are responsible for, and agree that:

- All research must be conducted in accordance with the protocol and all other study forms as approved in this submission. Any revisions to the approved study procedures or documents must be reviewed and approved by the IRB prior to their implementation. Please use the UD amendment form to request the review of any changes to approved study procedures or documents.
- Informed consent is a process that must allow prospective participants sufficient opportunity to discuss and consider whether to participate. IRB-approved and stamped consent documents must be used when enrolling participants and a written copy shall be given to the person signing the informed consent form.
- Unanticipated problems, serious adverse events involving risk to participants, and all non-compliance issues must be reported to this office in a timely fashion according with the UD requirements for reportable events. All sponsor reporting requirements must also be followed.

The UD IRB REQUIRES the submission of a PROGRESS REPORT DUE ON September 8, 2021. A continuing review/progress report form must be submitted to the UD IRB at least 45 days prior to the due date to allow for the review of that report.

If you have any questions, please contact the UD IRB Office at (302) 831-2137 or via email at hsrb-research@udel.edu. Please include the study title and reference number in all correspondence with this office.

Generated on IRBNet

Appendix C

INSTITUTIONAL REVIEW BOARD AMENDMENT APPROVAL 2

Institutional Review Board
210H Hullihen Hall
Newark, DE 19716
Phone: 302-831-2137
Fax: 302-831-2828

DATE: September 20, 2021

TO: Keith Schneider
FROM: University of Delaware IRB

STUDY TITLE: [1472937-4] Binocular rivalry
SUBMISSION TYPE: Continuing Review/Progress Report

ACTION: APPROVED
EFFECTIVE DATE: September 20, 2021
NEXT REPORT DUE: September 8, 2022

REVIEW TYPE: Administrative Review
REVIEW CATEGORY: Expedited review category # *(4,7)*

Thank you for your Continuing Review/Progress Report submission to the University of Delaware Institutional Review Board (UD IRB). The UD IRB has reviewed and APPROVED the proposed research and submitted documents via Administrative Review in compliance with the pertinent federal regulations.

As the Principal Investigator for this study, you are responsible for, and agree that:

- All research must be conducted in accordance with the protocol and all other study forms as approved in this submission. Any revisions to the approved study procedures or documents must be reviewed and approved by the IRB prior to their implementation. Please use the UD amendment form to request the review of any changes to approved study procedures or documents.
- Informed consent is a process that must allow prospective participants sufficient opportunity to discuss and consider whether to participate. IRB-approved and stamped consent documents must be used when enrolling participants and a written copy shall be given to the person signing the informed consent form.
- Unanticipated problems, serious adverse events involving risk to participants, and all non-compliance issues must be reported to this office in a timely fashion according with the UD requirements for reportable events. All sponsor reporting requirements must also be followed.

The UD IRB REQUIRES the submission of a PROGRESS REPORT DUE ON September 8, 2022. A continuing review/progress report form must be submitted to the UD IRB at least 45 days prior to the due date to allow for the review of that report.

If you have any questions, please contact the UD IRB Office at (302) 831-2137 or via email at hsrb-research@udel.edu. Please include the study title and reference number in all correspondence with this office.

INSTITUTIONAL REVIEW BOARD

74